CHALMERS

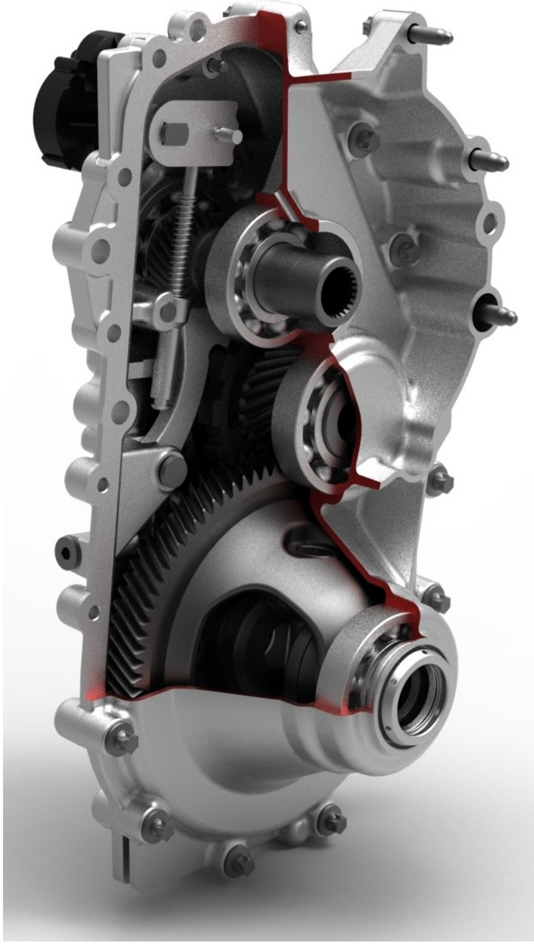

Gear Whine Noise Excitation Model

Master's Thesis in Mechanical Engineering

A. IVAR NILSSON

Department of Applied Mechanics
Division of Dynamics
Chalmers University of Technology
Gothenburg, Sweden 2013

Master's Thesis 2013:05

MASTER'S THESIS IN MECHANICAL ENGINEERING

Gear Whine Noise Excitation Model

A. IVAR NILSSON

Department of Applied Mechanics
Division of Dynamics

CHALMERS UNIVERSITY OF TECHNOLOGY
Gothenburg, Sweden 2013

Gear Whine Noise Excitation Model
A. IVAR NILSSON

Master's Thesis 2013:05
ISSN 1652-8557
Department of Applied Mechanics
Division of Dynamics
Chalmers University of Technology
SE-412 96 Gothenburg
Sweden
Telephone: +46 (0)31-772 1000

Cover:
Electrical vehicle transmission used as test object throughout this work. The transmission is developed by Vicura AB.

Chalmers Reproservice/Department of Applied Mechanics
Gothenburg, Sweden 2013

Abstract

When developing a mechanical transmission one important characteristic of the transmission is how much tonal noise and vibrations it generates. The vibrations causing the so called gear whine noise are generated in the gear contacts of the transmission and propagate through the shafts and bearings to the housing, where they become airborne. This is of extra concern in electrical vehicle applications, where the absence of a loud combustion engine makes the gear whine noise more distinct and easily perceived by the human ear.

In collaboration with Vicura AB, a dynamic finite element model of an electric vehicle transmission has been developed using the Abaqus® software in order to simulate the vibrations causing the gear whine noise. The main cause of the vibrations has been assumed to be excitations due to variations in the transmission error and the mesh stiffness of the gear contacts, based on previous studies of the subject. The transmission errors and mesh stiffnesses for the examined transmission have been calculated and implemented into the finite element model to excite the system. Dynamic simulations using reduced finite element models of the transmission were performed so that the resulting dynamic response in the transmission housing could be examined for a range of different operating conditions.

Results from the simulations indicated that the mesh frequencies of the gear drives along with their harmonics were the dominating frequencies in the response of the housing. Resonance phenomena were observed when the mentioned frequencies coincided with the eigenfrequencies of the transmission.

It could be concluded, based on the results from the simulations, that the developed dynamic model managed to simulate the vibrations established as the main cause of the gear whine noise. Experiments must however be performed in order to establish the validity of the model.

Keywords: *gear whine noise, transmission error, mesh stiffness, gear dynamics*

Acknowledgements

I would like to thank my supervisor Martin Johansson for his great help and guidance throughout this thesis. Many thanks to the staff at Vicura AB for their consistent help and sharing of knowledge. I would also like to give thanks to my examiner Peter Folkow for his input and mentoring.

Ivar Nilsson, Gothenburg 30/1-2013

Contents

Nomenclature

c	Damping coefficient
c_d	Center distance
c_m	Mesh damping
CR	Contact ratio
$e(t)$	Excitation
F_a	Axial force
f_m	Mesh frequency
f_{max}	Maximum frequency
F_n	Normal force
F_t	Transverse force
i	Gear ratio
k	Stiffness
k_m	Mesh stiffness
k_t	Torsional stiffness
M	Torque
m	Mass
n	Number of samples
p_b	Base pitch
r	Pitch radius
r_b	Base radius
t	Time
T	Total time
T_m	Time period of mesh cycle
TE_{ang}	Angular transmission error
TE_{lin}	Linear transmission error
x	Displacement
z	Number of gear teeth
β_b	Helix angle
θ	Angular position
ϕ	Pressure angle
ω	Angular velocity

1

Introduction

When developing a mechanical transmission one important noise, vibration and harshness (NVH) characteristic of the transmission is how much tonal noise and vibrations it generates. This noise is generated in the gear contacts due to variations in the so called transmission error, which can be described as an error in the gear ratio of a gear drive. Gear whine noise is a factor which becomes even more important when designing transmissions for electrical vehicles. In such applications, the noise generated from the transmission becomes more distinct since the noise level of the electric motor is much lower compared to an internal combustion engine. The gear whine noise is often recognized as the whining noise from F1 cars or reversing cars.

Several models for determining the resulting dynamic response due to the excitation of the transmission error, with varying level of complexity and accuracy have been proposed since the 1950's. The simplest models are single degree of freedom systems, while more complex models have an increasing number of degrees of freedom. Also, more detailed finite element models have been proposed to describe the interaction in the gear contacts.

This master thesis is performed in collaboration with the engineering company Vicura AB located in Trollhättan, Sweden. The main focus of Vicura AB is in mechanical transmissions, electric drive systems and related control systems. As noise levels are of increasing concern, an applicable model to describe the dynamic behavior of transmissions is of great interest.

1.1 Objective

The aim of this thesis is to investigate different ways to implement the excitation due to the transmission error and create a method or subroutine using the finite element analysis software Abaqus®, which applies the gear excitation to a dynamic finite element model of a transmission. Focus lies in finding a simple yet representative model of the gear contact. The dynamic response in the transmission should then be simulated, with focus in the response of the housing of the transmission. This is done in order to enable Vicura AB to examine the dynamic behavior of transmissions, so that tendencies in the expected level of gear whine noise can be estimated and compared between different transmission designs. Throughout this thesis, analyzes will be performed on a mechanical transmission developed by Vicura AB for the use in an electric vehicle. A more detailed description of the examined transmission is given in Section 1.3 below.

1.2 Limitations

To confine the scope of this thesis the following limitations have been introduced:

- Damping effects in the dynamic behavior of the models will not be considered. This limitation is introduced in order to simplify the modeling and will decrease the accuracy of the model.
- The representations of the transmission components will be so called substructures, which are reduced finite element models. These will be based on currently available models of the examined transmission.
- The dynamic response will be investigated only in the housing of the transmission, since it is from there the vibrations become airborne.
- Verification of the accuracy of the model by experimental measurements on the transmission will not be considered. This will be left for future work, since it is too extensive to be included in this thesis.

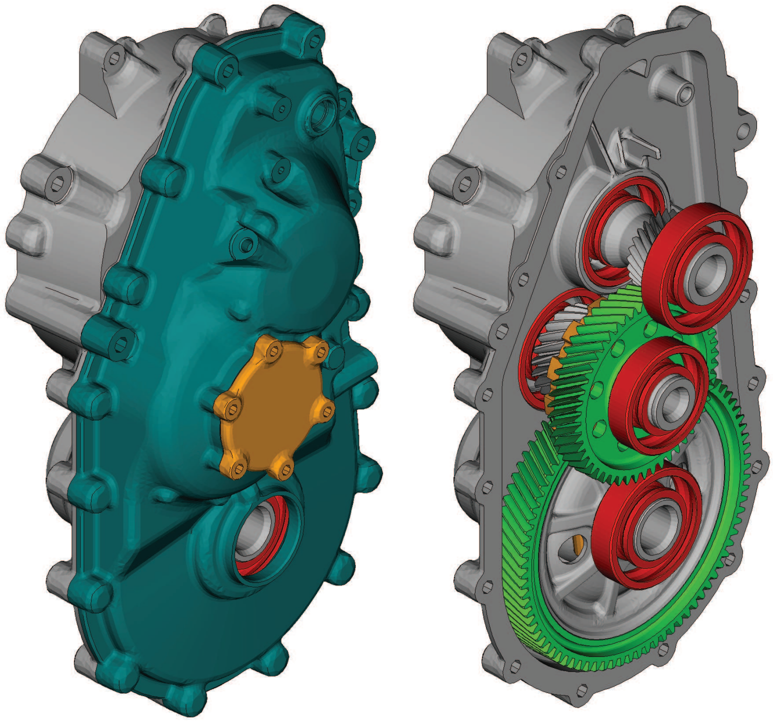

Figure 1.1: Illustrations of the transmission used throughout the thesis. The left image shows the outside of the transmission housing, while the right image shows the shafts and bearings inside the housing.

1.3 Description of the Examined Transmission

As mentioned in Section 1.1, the transmission used as test object for this thesis is designed for an electrical vehicle. The transmission has a constant overall gear ratio and has the function of transferring power delivered from the motor to the rest of the driveline while reducing the rotational speed and increasing the torque. An illustration of the transmission can be seen in Figure 1.1. Three shafts with attached gears are supported by ball bearings and covered by a housing. The topmost shaft is the input shaft which is connected to a motor, which is not shown in the figure. An intermediate shaft, called the main shaft, transfers the power from the input shaft to the differential, which can be seen in the bottom of the figure. The inner components of the differential are not included in the examined transmission along with the shafts connecting the differential to the remaining driveline. All of the bearings are single row, deep groove ball bearings. The housing of the transmission has a height of circa 450 mm, a width of circa 240 mm and a depth of circa 200 mm.

Figure 1.2 illustrates the shafts and the gear train of the transmission in greater detail. Four helical involute gears form two gear drives, which reduce the rotational speed from

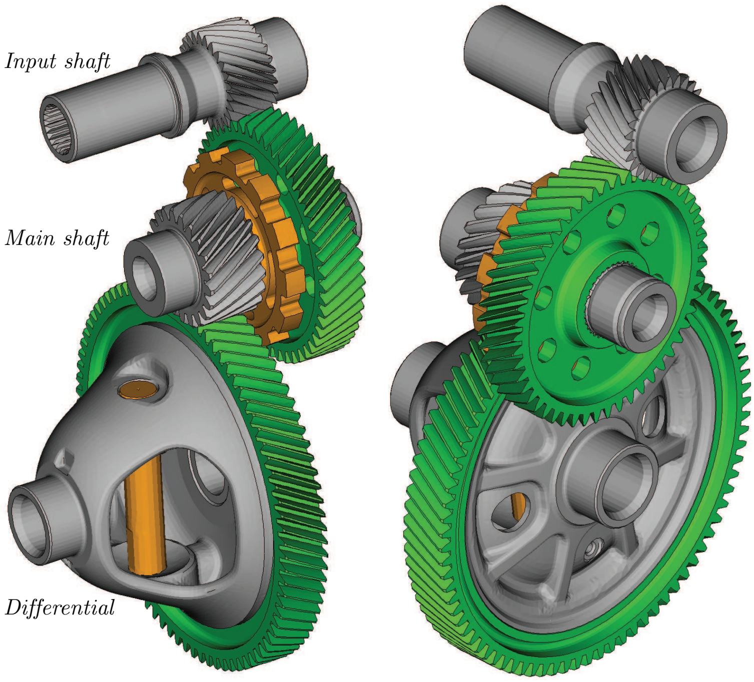

Figure 1.2: Illustrations of the transmission gear train. It can be seen that it consists of three shafts with two gear drives.

the motor in two steps. All gears have a helix angle of $\beta_b = 30°$, see Section 2.2 for definition of helix angle. The gear of the input shaft has $z_1 = 19$ gear teeth and is connected to the main shaft via a gear with $z_2 = 51$ teeth. This gear contact will be called the first gear contact throughout this thesis. The resulting gear ratio between the input shaft and the main shaft is thus $i_1 = z_2/z_1 \simeq 2.68$, see Section 2.2, indicating that the input shaft rotates 2.68 times faster than the main shaft. The main shaft then transfers the rotation to the differential via a gear with $z_3 = 23$ teeth which is connected to the differential gear having $z_4 = 83$ teeth. This results in a gear ratio of $i_2 = z_4/z_3 \simeq 3.61$ between the main shaft and the differential. The overall gear ratio of the transmission is thus $i = i_1 \cdot i_2 = 9.69$. The gear contact between the main shaft and the differential will be referred as the second gear contact throughout this thesis. The gear-like component between the two gears of the main shaft is used for a park lock which locks the transmission when the vehicle is parked and has no interaction in the gear train. Other components associated to the park lock are not included in the figure and has not been considered in the thesis work.

2

Review of Literature

This chapter will in greater detail explain the relevant theories and reviewed literature. Initially, the phenomena of gear whine noise will be discussed followed by basic theory regarding the geometry of involute gears. This is followed by a description of the forces acting between gears and the concept of transmission error and mesh stiffness. Thereafter follows a revision of different concepts for modeling the dynamics in gear contacts. The last section explains the method of fast fourier transform.

2.1 Gear Whine Noise

There are many types of different noises associated with gears, but one of the more distinct noises is the so called gear whine noise. This noise is emitted from gears that are in mesh and the sound is characterized as vibrations with frequencies same as the gear mesh frequency and its multiples [1]. The noise exhibits a periodic behavior and it is therefore perceived as a tonal noise. It is therefore an important factor when reducing the noise level of transmissions since the human ear is more sensitive to tonal noises, compared to noises with more random characteristics [2].

The primary cause of noise generation in gear transmissions are force variations which cause some of the mechanical components to vibrate [3]. These forces generally varies in amplitude, direction or position. The vibrations are then transmitted via the shafts through the bearings to the housing. This excites the housing from which airborne noise can be produced [3]. Vibrations are also transferred through the housing mountings where they can excite other external components, such as parts of the compartment in a vehicle. Previous studies [4] [5] [6] generally conclude that one of the main sources of excitation in geared systems is the so called transmission error, see Section 2.5 for a detailed description. The transmission error has also been identified as the primary cause of gear whine noise generation [7] [8].

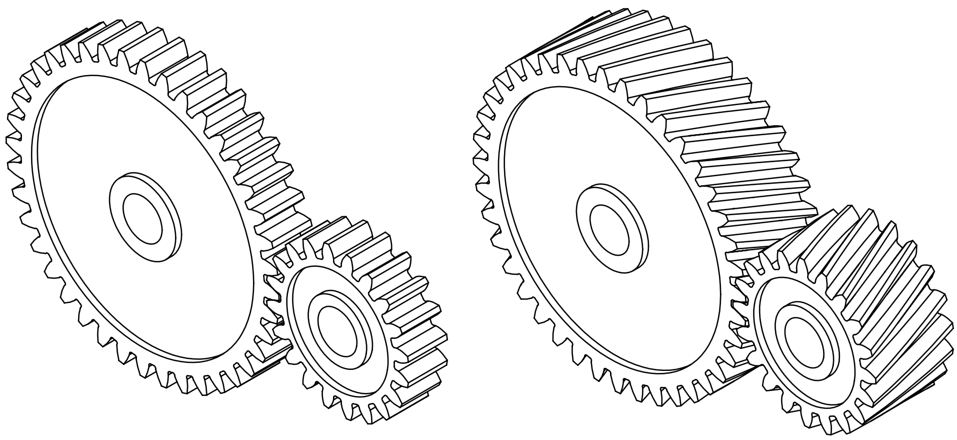

Figure 2.1: Two examples of parallel-axis gear drives. To the left is a spur gear drive and to the right is a helical gear drive.

2.2 Involute Gear Geometry

The primary function of gears is to transfer power between two shafts while maintaining a constant ratio in the velocities of the shaft rotations. Torque is transmitted via forces in the contact between the teeth of the driving and the driven gear and since the gears are rotating, power is transferred. There are different types of gear configurations but the simplest and most popular is the parallel-axis gear drive [9], which is shown in Figure 2.1. This configuration connects two parallel shafts and allows a relatively high amount of power transfer.

The primary gears used in a parallel-axis gear drive are spur gears and helical gears. Figure 2.1 shows the basic geometries of a spur and helical gear drive. The two gear types are similar but with one major difference; the spur gear has teeth which are parallel to the shaft axis, while the helical gear has teeth which follows a spiral around the shaft axis. The geometry of the helical gear is more complicated than that of the spur gear, but it has some advantages. The teeth gradually engage contact through the meshing cycle which results in a smoother and quieter action. Helical gears also allow for larger loads to be transmitted compared to spur gears, which implies that the life of the helical gear will be longer for the same load [9]. One disadvantage of the helical gear is that due to the twisting angle of the teeth, additional force components along the shaft are present. This requires extra considerations regarding the bearings of the shaft and the design of the gear housing [9]. Also, helical gears have a somewhat lower efficiency compared to spur gears [9].

The fundamental law of gearing states that in order to maintain a constant velocity ratio of the two meshing gear teeth, the common normal to the tooth profile at the point of contact must always pass through a fixed point, called the pitch point, which is located at the pitch circles of the two gears [9]. This criterion affects the possible shapes of the gear teeth. There are different gear profiles that fulfills this criterion but the most

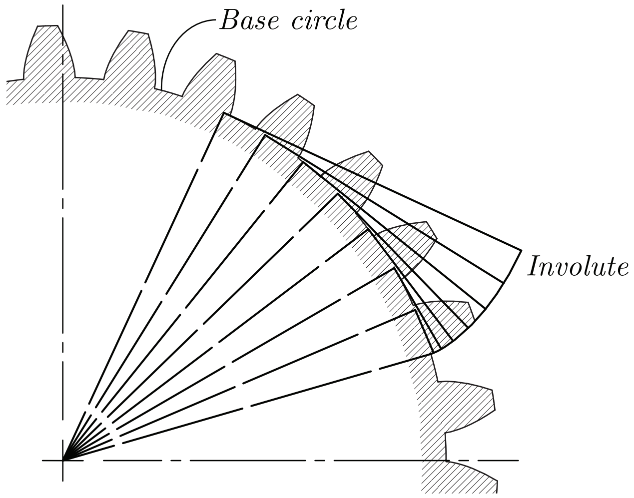

Figure 2.2: Generation of an involute curve used for the shape of the gear tooth. The involute curve can be imagined as the path of the end of a string unwinding from the base circle.

commonly occurring is the involute gear profile. The shapes of the two flanks of an involute gear tooth are based on the involute curve of a circle. This curve is generated by the movement of a point on the end of a taut string unwinding from a so called base circle [10]. The generation of an involute curve and the final shape of a corresponding involute gear tooth can be seen in Figure 2.2. Beyond the fulfillment of the fundamental law of gearing, the involute gear shape also allows for small deviations in the center distance of the gears without changing the transmission ratio [10].

A principle sketch of two spur gears in mesh can be seen in Figure 2.3. The sketch illustrates the pitch point, p_p, the pressure angle, ϕ, and the pitch and base circles of the two gears. The pitch point is as described above the point through which the contact forces between the teeth of the two gears pass. Between point a and b is the so called line of action. This line is tangent to both of the base circles of the gears and all contacts between the teeth of the spur gears occur along this line. The normal forces in the tooth contacts are all directed along the line of action due to the involute shape of the teeth [10]. The pressure angle is defined as the angle between the line of centers and a line perpendicular to the line of action and hence describes the direction of the normal forces in the tooth contacts. The radii of the pitch circles, r_1 and r_2, are defined from the distance between the centers of the gears, c_d, and the gear ratio of the gear drive according to [10]

$$r_1 = \frac{c_d}{\frac{z_2}{z_1} + 1} \tag{2.1}$$

$$r_2 = \frac{c_d}{\frac{z_1}{z_2} + 1} \tag{2.2}$$

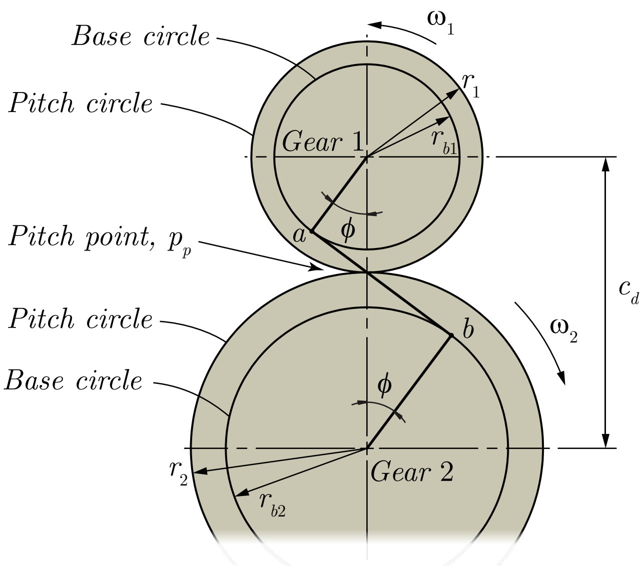

Figure 2.3: Sketch of a spur gear drive showing pitch and base circles, pitch point and pressure angle ϕ.

where z_1 and z_2 are the number of teeth for Gear 1 and Gear 2 respectively and the fraction z_2/z_1 is identified as the gear ratio, i. The gear ratio can also be expressed in terms of the base or pitch radii according to [10]

$$i = \frac{r_{b2}}{r_{b1}} = \frac{r_2}{r_1} \tag{2.3}$$

or in angular velocities as

$$i = \frac{\omega_1}{\omega_2} \tag{2.4}$$

where ω_1 and ω_2 are angular velocities of Gear 1 and Gear 2 respectively. The radii of the base circles are obtained from the pressure angle and the pitch circle radius according to [10]

$$r_{b1} = r_1 \cos\phi \tag{2.5}$$

$$r_{b2} = r_2 \cos\phi \tag{2.6}$$

Another important geometrical definition is the base pitch of a gear, p_b. It is defined as the distance measured along the base circle from one point on one tooth to the corresponding point on an adjacent tooth. For two mating gears the base pitch of the gears are identical and it can be expressed as [10]

$$p_b = \frac{2\pi r_{b1}}{z_1} = \frac{2\pi r_{b2}}{z_2} \tag{2.7}$$

The geometry of a helical gear follow similar standards as those for the spur gear. Instead of having teeth which are parallel to the axis, the teeth wind around the axis

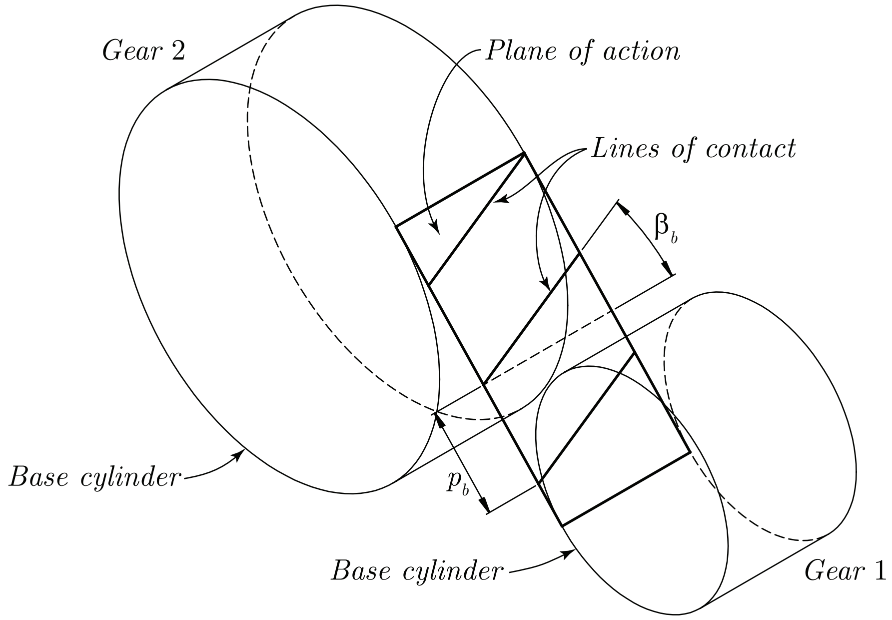

Figure 2.4: The plane of action and contact lines between two mating helical gears.

helically similar to the threading of a screw. If the geometry of the helical gear is examined in a sectional cut perpendicular to the axis of the gear, the profile is found to be identical to that of a corresponding spur gear [10]. The helix which the teeth is wind along is usually described by an angle measured at a tangential plane to the rotational axis of the gear. The angle varies with the radius to the tangential plane and it is therefore common to use the helix angle at the tangential plane to the base circle, β_b. Typical values for this helix angle is between 0° and 45°.

For a helical gear the contact between the gear teeth occur at a plane which is tangent to the base cylinders of the two mating gears. This plane is illustrated in Figure 2.4. It can be seen that the teeth of the gears are in contact along lines with an angle of β_b and at distances equal to the base pitch, p_b [10]. The contact lines migrates along the plane of action from the base cylinder of one gear to the one of the other, but always with the constant angle of β_b.

2.3 Contact Ratio of Involute Gears

When two gears are working together the number of gear teeth which are in contact varies during the meshing cycle. In order for the gear drive to work properly there must be at least one pair of teeth in contact at all times. The average number of gear teeth in contact when the gears are operating is called the contact ratio, CR. In practice the contact ratio varies between two discrete values and a contact ratio of e.g. CR = 1.3 describes that some of the time there is one gear tooth pair in contact and for the rest of the time there are two pairs in contact. Acceptable values for the contact ratio is usually CR > 1.2 with a absolute minimum of CR $= 1.1$ [9] [11]. If a contact ratio below this value occurs, correct motion transfer cannot be assured [10].

2.4 Forces in Helical Gears

The pressure which is acting on the tooth surface of a helical gear when transferring torque can be approximated by a resultant force denoted F_n acting in the normal direction to the tooth surface [10]. This is based on the neglecting of the relatively small friction forces which arise due to the slipping between the gear teeth flanks. Due to the helix angle, this resultant force can be divided into two force components; one transverse force component F_t and one axial force component F_a. This is illustrated in Figure 2.5. The components are obtained using the following expressions [10]

$$F_t = F_n \cos\beta_b \tag{2.8}$$

$$F_a = F_n \sin\beta_b \tag{2.9}$$

It is the transverse force component which transfers the desired torque from the driver gear to the driven gear, while the axial component is a result from the twist of the gear tooth profile. According to Equation 2.11 it can be seen that the axial force component increases as the helix angle increases. If an input torque, M_1, is applied to Gear 1 in Figure 2.5, the transverse force can be expressed as [10]

$$F_t = \frac{M_1}{r_{b1}} \tag{2.10}$$

From geometry the axial force component can then be expressed in terms of the input torque as

$$F_a = \frac{M_1}{r_{b1}} \tan\beta_b \tag{2.11}$$

The resulting output torque of Gear 2 can easily be derived using the gear ratio between the two gears according to [10]

$$M_2 = M_1 \cdot i \tag{2.12}$$

2.5 Transmission Error and Mesh Stiffness

In theory, the shape of involute gears should result in a constant ratio in the rotational speeds of two mating gears, i.e. a constant rotational speed in the input shaft of a gear drive would result in a constant rotational speed in the output shaft [12]. This is based on the assumption that the gears are perfectly rigid and that there are no geometrical errors present. However, in reality gears are elastic [3] and geometrical errors are to some extent inevitable which will result in variations in the ratio of the rotational speeds of the gears. To describe these deviations in the rotational speeds the transmission error have been introduced. A formal definition of transmission error is [12]

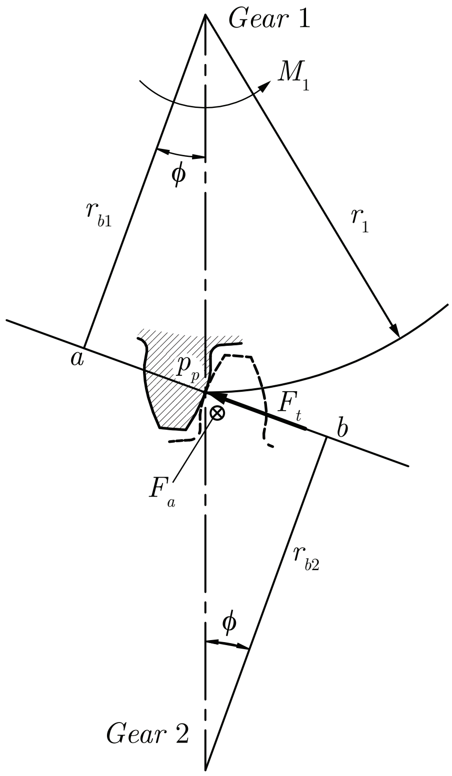

Figure 2.5: Force components acting on a gear tooth when a torque, M_1, is applied to Gear 1.

> *"The difference between the actual position of the output gear and the position it would occupy if the gear drive were perfectly conjugate"*

This difference can be expressed as an angular displacement in the position of the two gears according to

$$\mathrm{TE}_{ang} = \theta_1 - \frac{r_{b2}}{r_{b1}}\theta_2 \tag{2.13}$$

or as a linear displacement [13] along the line of action according to

$$\mathrm{TE}_{lin} = r_{b1}\theta_1 - r_{b2}\theta_2 \tag{2.14}$$

where r_{b1} and r_{b2} are the base radii and θ_1 and θ_2 are the angular positions of Gear 1 and Gear 2 respectively, see Figure 2.6.

The transmission error depends greatly on the torque being transferred by the gear drive. Higher torque will cause a greater deformation of the gear teeth and thus a larger difference between the actual and conjugate position of the driven gear.

As discussed above in Section 2.3, the number of gear tooth pairs which are in contact varies during the mesh cycle of a gear pair. Since the gear teeth are elastic, this results

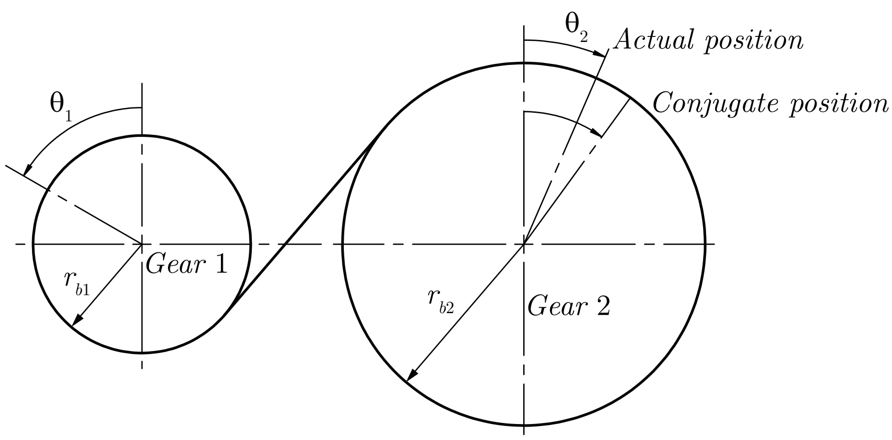

Figure 2.6: Illustration of the definition of transmission error.

in a variation in the stiffness of the gear mesh depending on where in the meshing cycle the gears are. The mesh stiffness is denoted k_m and can be defined as the load applied to a gear mesh divided by the resulting total deflection of the gear mesh. In the meshing cycle, when the higher number of gear teeth are in contact the torque transmitting force is distributed among a higher number of teeth. The resulting total deflection of the gear is therefore lower since the mesh stiffness of the gear is higher. When instead the lower number of teeth are in contact the force is distributed on a lower number of teeth which results in a higher deflection and hence the mesh stiffness is lower.

It can easily be realized that it is desirable to have a low transmission error in a gear drive. More specific, it is desirable to have a low variation in the transmission error, since it is the variations which can give rise to vibrations. The most common way to reduce the transmission error is by slightly modify the geometry of the gear teeth to compensate for the deformations. Such methods include so called lead crowning, profile crowning, helix angle modification and tip and end relief [12], and will not be treated in further detail in this work.

2.6 Mathematical Models Describing Gear Dynamics

This section discusses some of the proposed models to describe the dynamic behavior of gears. The first part explains the models developed and refined in order to describe the interaction in the contact of a gear pair. For the second part different ways to model the system surrounding the gears, including bearings and housing, are reviewed.

2.6.1 Gear Contact Models

A simple model describing the contact between two gears was proposed by Tuplin [14] in 1950. He described a pair of spur gears as two rigid bodies connected through a spring

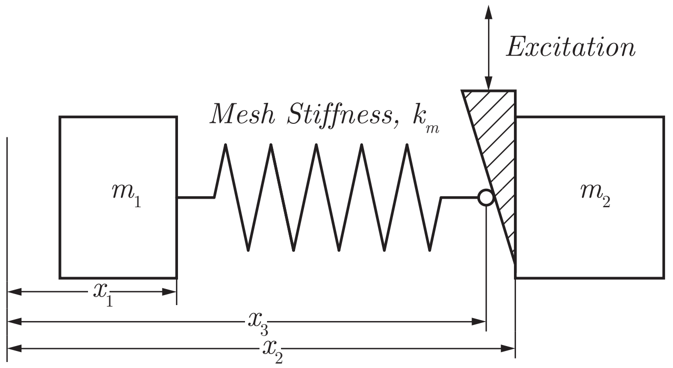

Figure 2.7: Dynamic model proposed by Tuplin [14] in 1950, describing the contact between two gears. The relative displacements of the equivalent masses, m_1 and m_2, of the two gears are denoted x_1 and x_2 respectively, while the error is defined as $x_2 - x_3$.

with constant stiffness, see Figure 2.7. The spring represented the torsional flexibility in the connection of the two mating gears. The bodies were given the equivalent masses of the corresponding gears and their associated rotating masses at the pitch point. These equivalent masses were calculated as the total moment of inertia for each of the gears, divided by the square of their respective pitch radius. Gear errors were then introduced as a source of excitation by the insertion and removal of a wedge between the spring and one of the equivalent masses according to Figure 2.7. The main application of the model was to evaluate the magnitude of the dynamic loading occurring from geometrical errors in order to estimate the maximum stresses in the gear teeth.

A refinement of the model described above was discussed by Gregory et al. [4] in 1962. The configuration of this model can be seen in Figure 2.8. Two spur gears considered as rigid disks were connected by a spring which were attached to the base circles of the each respective gear. The spring was thus acting along the line of action of the two gears, see Section 2.2. A proposed transmission error for the gear drive was introduced and expressed as a linear displacement along the line of action. This resulted in one effective degree of freedom within the system corresponding to the transmission error. The stiffness of the spring was modeled as time variant, depending on the number of gear teeth in contact.

A model described by Singh et al. [5] in 1990 combined the mesh stiffness along with a viscous damping. It also included the transmission error as a time dependent displacement excitation in the gears. The model is illustrated in Figure 2.9. The mesh stiffness used was assumed to be time invariant but effects of backlash in the gears was taken into account. This was implemented by setting the mesh stiffness equal to zero when the gears ceased to be in contact and otherwise constant.

Further advanced models involves finite element modeling of the gear contact, such as one proposed by [15]. Two gears in mesh were analyzed by using a fine computational mesh, resolving the teeth of the gears. Different models of the gear contact with different

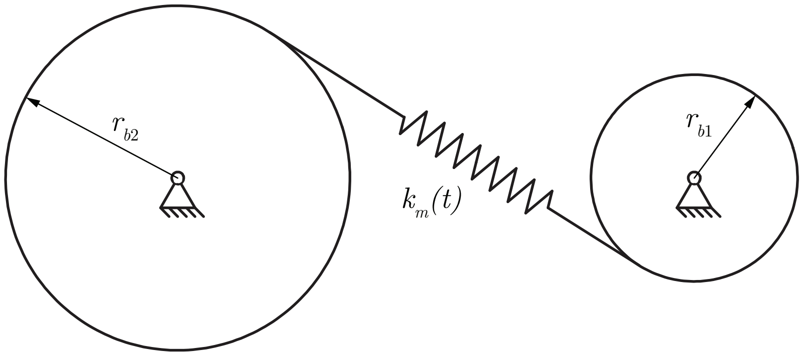

Figure 2.8: Dynamic model proposed by Gregory et al. [4]. The model consists of two rigid discs representing gears connected by a time variant mesh stiffness, $k_m(t)$.

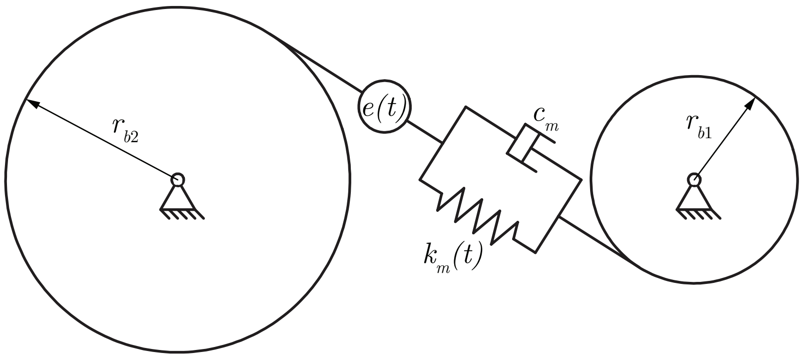

Figure 2.9: Dynamic model proposed by Singh et al. [5]. The model contains an excitation due to the transmission error, $e(t)$, a time variant mesh stiffness, $k_m(t)$ and a viscous mesh damping, c_m.

levels of complexity was used to describe the interaction between the two gears, some which also included sliding friction between the gear teeth.

2.6.2 Gear Drive System Models

In order to simulate the dynamic response of the shafts and the housing of a transmission due to excitations in the gear contacts, models describing the dynamic behavior of the shafts and the bearings can be used. Simple analytical models describe the gears and shafts as rigid bodies with lumped masses and inertias, and implement the lateral stiffness and damping of shafts and bearings as springs and dampers connecting the shafts to a rigid housing. Consideration to torsional vibrations can be included by representing the torsional stiffness of the shaft by torsional springs connecting the gears to the bearing points [16]. An illustration of such a model can be seen in Figure 2.10. This type of model with slight modifications has been proposed for several analytical dynamic analyzes of

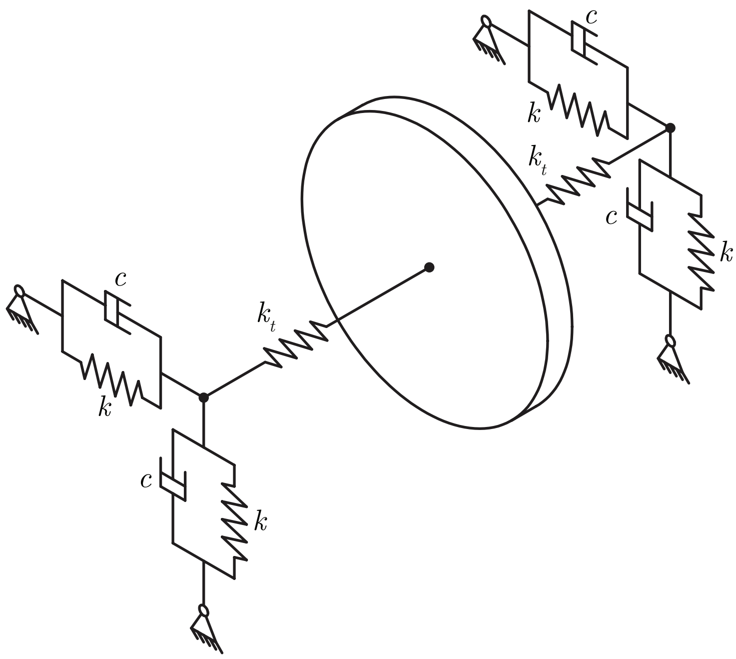

Figure 2.10: Example of mathematical model describing a shaft with an attached rigid gear supported by bearings. The shaft has a torsional stiffness of k_t and the bending stiffness of the shaft and the stiffness of the bearings are represented by springs with stiffness k, connecting the shaft to the housing. Also, damping effects in the bending of the shaft in the bearings are represented by dampers with a damping coefficient of c.

geared systems e.g. [17] [18] [19] [20]. The most common way to change the complexity of the model is by increasing and decreasing the number of degrees of freedom.

Further refinement of the system model can be obtained by describing the shafts as continuous, flexible beams. Thereby the different eigenmodes of the shafts can be considered in dynamical analyzes of the model [16].

By using the finite element method, complex continuous systems including the shafts, bearings and housing can be discretised so that the system's dynamic behavior can be simulated [16]. The eigenmodes and corresponding eigenfrequencies can thereby be obtained for the entire system.

2.7 Substructuring in Abaqus

When using a number of parts with relatively fine meshes connected together in a finite element model, the total number of degrees of freedom can easily reach high values, resulting in expensive analyzes regarding computational time and resources. A simplified version of the model can be obtained by using so called substructures in Abaqus®. A substructure is a representation of a part, but with all degrees of freedom excluding those necessary to connect the part to the other parts eliminated. The finite elements of the part are collected into the substructure whose response is defined by the stiffness, mass and damping matrices of the retained degrees of freedom [21]. These matrices connect the retained degrees of freedom and describe the response within a substructure as a linear perturbation about the original state of the substructure [21].

In order to better approximate the dynamic behavior of the substructure, generalized degrees of freedom associated with the natural modes of the part being reduced can also be included using dynamic mode addition. In Abaqus®, three different types of eigenmodes can be included;

- Fixed-interface eigenmodes using the Craig-Bampton method.
- Free-interface eigenmodes using the Craig-Chang method.
- Mixed-interface eigenmodes.

All of these methods are explained thoroughly in e.g. [22]. If the fixed-interface eigenmodes are used, all of the retained degrees of freedom of the part are fixed when the eigenmodes are evaluated. For the case of free-interface eigenmodes, all of the retained degrees of freedom are instead unconstrained. If some of the retained degrees of freedom are constrained and others are free, the mixed-interface eigenmodes are used. However, using the latter approach the time consumption for the generation of the substructure can increase greatly.

Practically, in Abaqus® a substructure is obtained by processing each part individually before any simulation of the system containing the substructures is performed. A frequency analysis to obtain the eigenmodes and eigenfrequencies of the part is also necessary if mode addition is to be used. Once a substructure has been generated, it can be used for many analyzes without repeating the generation process.

2.8 Fast Fourier Transform

According to Fourier series theory, a periodic signal can be expressed as an infinite series of sine and cosine terms, or alternatively an infinite series of complex exponential terms [22]. Each of these terms has a frequency which is a integer multiple of the fundamental frequency of the original signal which are called the harmonics of the signal. A periodic signal or function of time with period T can be expressed as a fourier series according to [16]

$$f(t) = a_0 + \sum_{n=1}^{\infty} \left(a_n \cos \omega_0 n t + b_n \sin \omega_0 n t \right) \tag{2.15}$$

where $\omega_0 = 2\pi/T$ is the fundamental frequency of the signal or function and the constants a_n and b_n are defined as [16]

$$a_n = \frac{2}{T} \int_0^T f(t) \cos \omega_0 n t \, \mathrm{d}t, \qquad b_n = \frac{2}{T} \int_0^T f(t) \sin \omega_0 n t \, \mathrm{d}t \tag{2.16}$$

for $n \geq 1$ and a_0 as

$$a_0 = \frac{1}{T} \int_0^T f(t)\, \mathrm{d}t \tag{2.17}$$

It can also be expressed in complex exponential terms as

$$f(t) = \Re \left(\sum_{n=0}^{\infty} c_n e^{\jmath \omega_0 n t} \right) \tag{2.18}$$

where the complex constants c_n are defined as [16]

$$c_n = a_n - \jmath b_n \tag{2.19}$$

If a signal instead is non-periodic, the Fourier series cannot be used. Instead the so called Fourier integral is used [22]. The non-periodic signal is then considered as a periodic signal with infinitely long period and Equations 2.18 and 2.19 become [16]

$$x(t) = \frac{1}{2\pi} \int_{-\infty}^{\infty} X(\omega)\, e^{\jmath \omega t}\, \mathrm{d}\omega \tag{2.20}$$

$$X(\omega) = \int_{-\infty}^{\infty} x(t)\, e^{-\jmath \omega t}\, \mathrm{d}t \tag{2.21}$$

These two equations are called a Fourier transform pair [22]. Both $x(t)$ and $X(\omega)$ are continuous functions and $X(\omega)$ contains all of the frequency components of the signal $x(t)$. $X(\omega)$ is therefore called the frequency spectrum of $x(t)$. Knowing the continuous signal $x(t)$, its composing frequencies can thereby be obtained using Equation 2.21 and vice versa using Equation 2.20.

If the signal $x(t)$ is obtained e.g. as output from a time simulation, it is not a continuous function. Instead it is a series of discrete real values. The frequency components of the signal can then not be obtained using the Fourier transform and instead the so called discrete Fourier transform (DFT) is used. This is defined as [16]

$$X_k = \sum_{r=0}^{n-1} x_r e^{-\jmath 2\pi k r / n}, \quad k = 0,1,2,\ldots,n-1 \tag{2.22}$$

and the inverse discrete Fourier transform according to

$$x_r = \frac{1}{n} \sum_{k=0}^{n-1} X_k e^{\jmath 2\pi k r / n}, \quad r = 0,1,2,\ldots,n-1 \tag{2.23}$$

where n is the number of equally spaced samples. If the time interval between the samples is Δt, then the total sample time is [22] $T = n\Delta t$. The frequency components in the DFT are then at intervals [22]

$$\Delta f = \frac{1}{T} = \frac{1}{n\Delta t} \tag{2.24}$$

The components of the DFT are not independent since X_{n-k} is the complex conjugate of X_k for $k = 1,...,n/2 - 1$ [16]. Therefore, the frequency spectrum only covers the range 0 to $(n/2)\,\Delta f$ and consists of $n/2 + 1$ frequency components.

The DFT requires n^2 complex multiplications for a sample of size n [16]. For increasing sample sizes, this rapidly turns into a slow operation. An algorithm known as the fast Fourier transform (FFT) reduces the number of mathematical operations required in order to perform the DFT of a sample. By using a sample size which is an integer power of 2, the FFT reduces the number of required complex multiplications to $(n/2)\log_2 n$ [16].

One problem with the DFT and FFT is that frequencies above $1/\,(2\Delta t)$, also known as the Nyquist frequency, appear at frequencies below the Nyquist frequency [16]. This problem is called aliasing and is avoided by using a sufficiently high sample frequency. Another problem is that if the sampled data contains a frequency component which does not precisely match a component in the DFT frequency spectrum, it will be spread between adjacent frequency components in the DFT [16]. This phenomenon is called leakage and is difficult to avoid entirely.

By using the FFT, sampled data e.g. the dynamic response of a transmission, can be described by the frequencies and their amplitudes constituting the response.

3

Method

The following chapter will explain the methodology of the development of the models used to simulate the dynamics of the transmission. Firstly, the finite element models used to represent the components of the transmission in the simulations will be described in detail. Thereafter follows a description of the process of calculating relevant transmission errors and mesh stiffnesses for the gear contacts. Finally, the methodology used for the post processing of the simulation results will be explained. It should be noted that for all simulations, effects of damping and friction have been neglected in order to simplify the models.

3.1 Development of Dynamic Model

In order to investigate the dynamic behavior giving rise to gear whine noise, a dynamic model of the transmission was developed using the Abaqus® software. This model was based on existing finite element models used by Vicura AB when performing static analyzes of the transmission. However, these models had to be modified to enable the dynamics of the transmission to be investigated.

The general procedure used for the construction of the dynamic model is illustrated in Figure 3.1.The first step in the development of the dynamic model was to modify the existing finite element models to introduce dynamic behavior. The models were then reduced into so called substructures, representing the components with only a few nodes connected by stiffness and mass matrices along with a number of eigenmodes, see Section 2.7 regarding substructures. The substructures were then assembled and connected by specially developed elements describing the interaction in the gear contacts and in the bearings. A model containing reduced models of the transmission components was then obtained and could be used for dynamic analyzes of the transmission. The main reason for using reduced finite element models is that the computational time of the simulations is greatly reduced, due to the great reduction in the number of degrees of

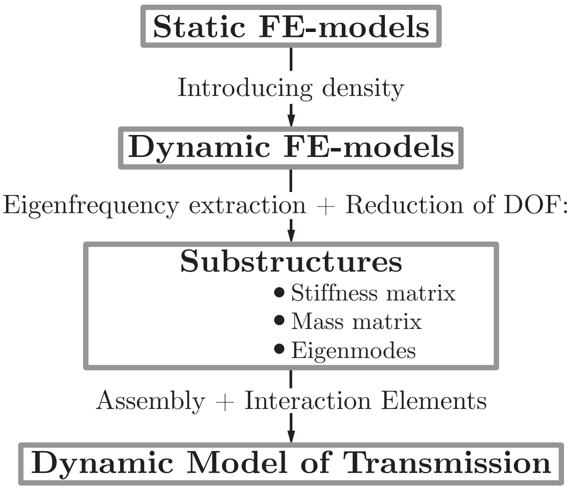

Figure 3.1: Flow chart describing the steps in the development of the dynamic model.

freedom. The following sections will describe the different models used for the dynamic simulations in greater detail.

3.1.1 Finite Element Models

The existing finite element models describing the transmission constituted of four components; input shaft, main shaft, differential and housing. The inner rings of the bearings were included in the shaft models, while the outer rings of the bearings were included in the housing model. Elasticity and thermal expansion coefficient for the component materials were defined previously but density definitions had to be added. All of the models had a relatively fine computational mesh since they were mainly used in static analyzes to estimate stresses and displacements in the components. Below follows a more detailed description of the finite element models used for the dynamic simulations.

Input Shaft

Images of the finite element model used to approximate the input shaft can be seen in Figure 3.2. The model consisted of a hollow shaft with an attached gear. The inner rings of the two ball bearings supporting the input shaft from the housing were included and connected to the shaft. The entire model consisted of tetrahedron elements. These were of type C3D10 in Abaqus®, and are categorized as quadratic, three-dimensional, solid, continuum elements with 10 nodes [21]. The total number of elements used for the input shaft model was 41,703 elements and the number of nodes was 74,430 nodes.

The model also contained four so called distributing couplings. These were used to equally distribute loads applied in one reference node, to a large set of nodes. For the bearings, the nodes on the surface of the inner bearing rings were connected to two reference nodes positioned in the middle of the bearing rings (50011 and 50012),

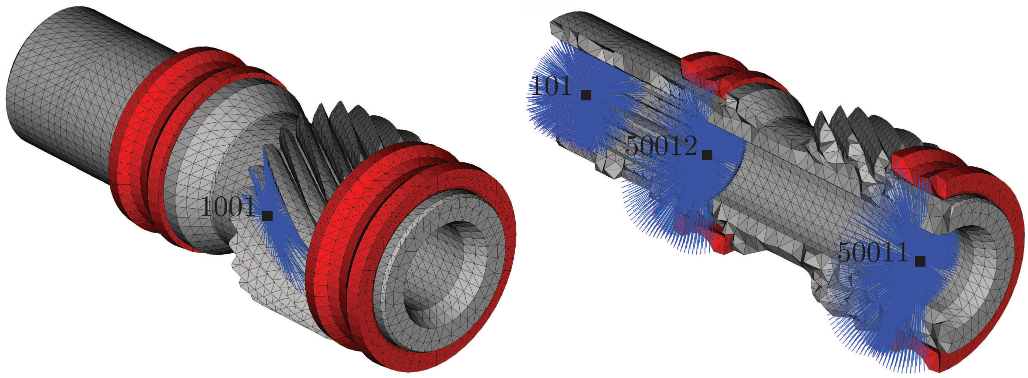

Figure 3.2: Finite element model used for the input shaft. The left image illustrates the distributing coupling used for the gear contact. The right image shows a sectional cut of the shaft and illustrates the distributing couplings used for the inner bearing rings and the spline coupling.

coincident to the center axis of the shaft. This is illustrated in Figure 3.2, which shows the distributing couplings used for the input shaft. The couplings are illustrated by lines connecting the surface nodes of the bearing rings to the reference nodes and a close-up of the couplings can be seen in Figure 3.3. The reason for the use of distributing couplings was that they allowed interactions between the inner and outer ring of the bearings to be described by a special bearing element connecting the reference nodes of the inner and outer bearing rings, see Section 3.1.5.

Another distributing coupling was used for the spline coupling where the input shaft is connected to the motor. Here, the distributing coupling was used to allow a prescribed load at a reference node (101) coincident to the center axis of the shaft, to be distributed to the splines. This enabled the torque from the motor to be applied to the input shaft by specifying it only at the reference node. The last distributing coupling was used to distribute the gear contact forces applied to a reference node (1001) to the surface nodes of two gear teeth. The reference node was located at the pitch point of the first gear drive in the transmission.

All elements in the model were given material properties of steel with a Young's modulus of $210 \cdot 10^3$ N/mm^2 and a density of $7.85 \cdot 10^{-9}$ tonnes/mm^3. The total mass of the input shaft was $9.5988 \cdot 10^{-4}$ tonnes.

Main Shaft

The finite element model used for the main shaft was similar to the one of the input shaft. Figure 3.4 shows the computational mesh used to approximate the main shaft. It can be seen that it consisted of a hollow shaft with two attached gears, a parking brake gear and the inner rings of the two ball bearings supporting the main shaft from the housing. As for the input shaft, the main shaft was represented by C3D10 tetrahedral

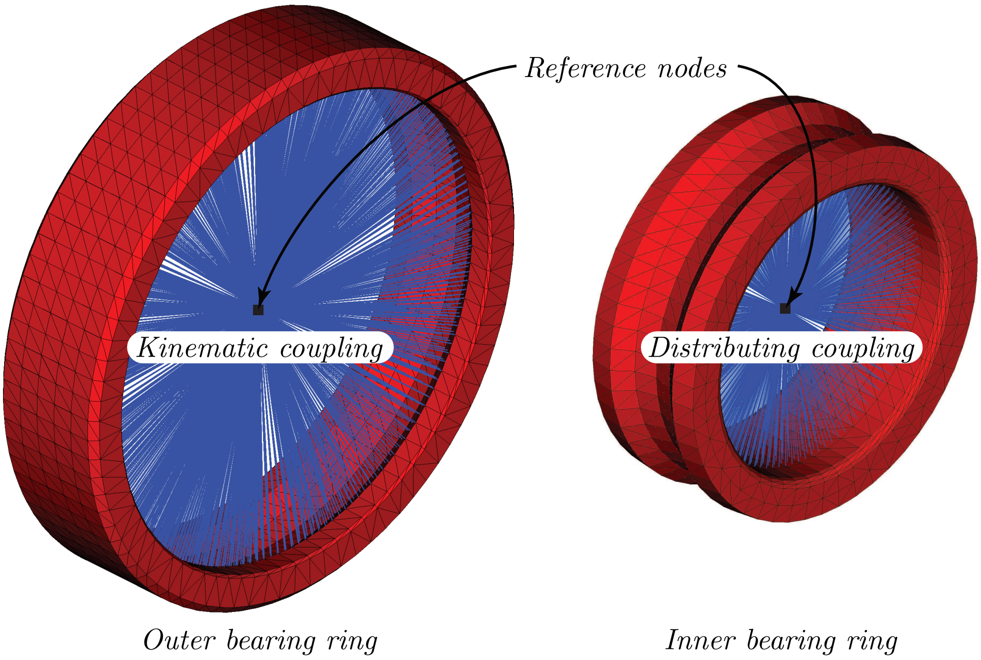

Figure 3.3: Illustration of the distributing and kinematic couplings used for the outer and inner bearing rings. The image to the left shows the kinematic coupling used for the outer bearing rings, while the right image shows the distributing coupling used for the inner bearing rings.

elements and the total number of elements used was 121,732 elements. The total number of nodes used was 215,347 nodes.

Distributing couplings were also used for the bearing rings of the main shaft. Two distributing couplings connecting the inner bearing rings to two reference nodes (50021 and 50022) coincident to the center axis of the main shaft was used. Similar to the input shaft, distributing couplings were also used to gather the nodes in the gear contacts to two reference nodes (2001 and 2002). These were located at the pitch points of the first and second gear drive.

The material of the main shaft elements was steel with the same properties as for the input shaft elements. The total mass of the main shaft was $2.6664 \cdot 10^{-3}$ tonnes.

Differential

The finite element model of the differential only included the carrier and the ring gear of the differential. It did not contain the bevel gears which should have been positioned inside the carrier but the shaft for the bevel gears was included. Figure 3.5 shows the model used for the differential. It can be seen that the model consisted of a carrier with an attached ring gear. Also the inner rings of the ball bearings used to support the

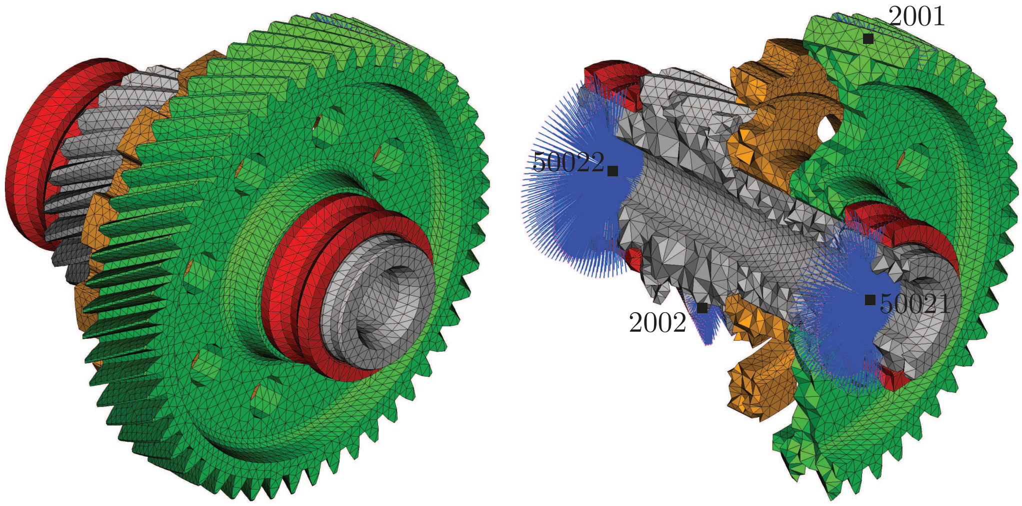

Figure 3.4: Finite element model used for the main shaft. To the left is an illustration of the overall configuration of the model. To the right is a sectional cut of the shaft, showing the distributing couplings used for the two inner bearing rings and the two gear contacts of the main shaft.

differential from the housing were attached to the carrier. The elements used for the differential were also of the C3D10 type and the number of elements used were 171,809 elements and the number of nodes was 298,775 nodes.

As for the other models described above, distributing couplings were used for the inner rings of the ball bearings. The two reference nodes (50031 and 50032) were located at the centers of respective bearing ring, coincident to the center axis of the differential. For the ring gear a distributing coupling was used as in the other models, in order to obtain one reference node (3002) for the gear teeth nodes exposed to contact with the gear of the main shaft. This reference node was located at the pitch point between the ring gear and the mating gear of the main shaft. Also a distributed coupling was used to connect the shaft for the bevel gears to one reference node (301). This enabled easy specification of boundary conditions for the differential. By specifying a zero displacement of reference node 301, a resulting torque would arise from the differential, to counter the applied input torque.

For the differential, two materials were used. The carrier was defined as a cast iron with a Young's modulus of $170 \cdot 10^3$ N/mm^2 and a density of $7.1 \cdot 10^{-9}$ tonnes/mm^3. The other parts of the differential was defined as steel with material properties same as for the input shaft. The total mass of the differential was $4.3867 \cdot 10^{-3}$ tonnes.

Housing

The finite element model used for the housing can be seen in Figure 3.6. The housing mainly consisted of two large models connected together, enclosing the gear drives and

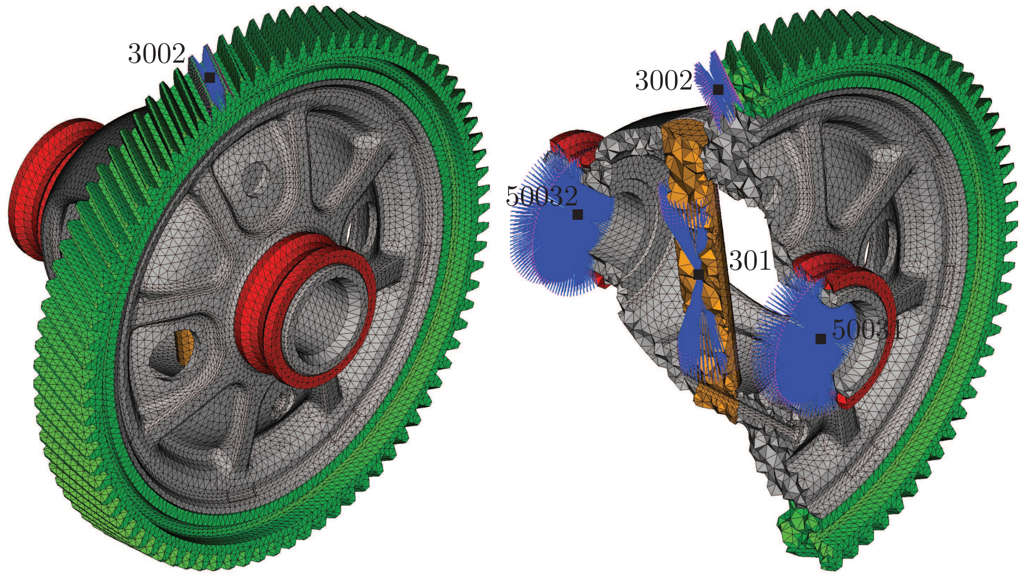

Figure 3.5: Finite element model used for the differential. The left image shows the whole of the model while the right image shows a sectional cut of the model. The distributing couplings used for the inner bearing rings and the gear contact and their respective reference nodes can be seen in the right image. Also, the distributing coupling for the bevel gear shaft and its reference node can be seen in the sectional cut.

the shafts. The outer bearing rings for all of the ball bearings supporting the shafts were included and attached to the housing. No screws or fasteners were included in the model. Instead, parts which should be fastened together were tied tightly together in the model. For the housing, elements of type C3D4 were used. These are tetrahedral elements similar to the C3D10 elements, but with 4 nodes instead of 10, thus making it a linear element instead of quadratic [21]. The use of linear elements is likely to increase the stiffness of the housing structure and may therefore result in e.g. higher eigenfrequencies, compared to instead using quadratic elements. However, by using linear elements the number of degrees of freedom is greatly reduced, resulting in less computational time needed during the substructure generation process, see Section 3.1.3. For the outer bearing rings the C3D10 elements were used. The total number of elements used for the housing model was 348,969 elements and the number of nodes was 161,809 nodes.

For the outer bearing rings so called kinematic couplings were used, see Figure 3.3. These create a rigid motion connection between a reference node and a set of nodes. Reference nodes (60011, 60012, 60021, 60022, 60031 and 60032) were introduced in the middle of each bearing ring and connected to the nodes of the inner surface of the bearing

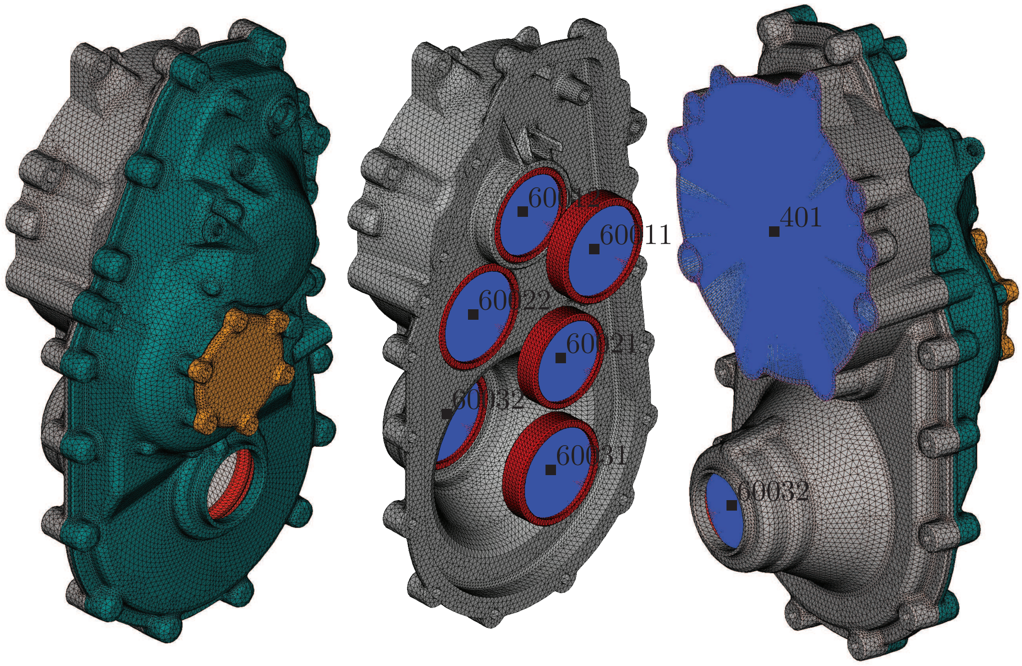

Figure 3.6: Finite element model used for the housing. The left image illustrates entire housing model, while the middle image shows the outer bearing rings attached to the inside of the housing. Kinematic couplings used for the bearing rings and their reference nodes are also shown. The right illustration shows the mounting surface for the attachment of the transmission to the motor, with the kinematic coupling used for the mounting surface and its reference node.

rings. The displacement of the inner surface of each outer bearing ring could thereby be described by the displacement of a reference node.

The nodes of the attachment surface of the housing to the motor was connected by a kinematic coupling to a reference node (401) in the center of the surface. This coupling was used to fix the housing by prescribing the displacement of the reference node and thereby prescribing the displacements for all of the surface nodes connected to the reference node. The attachment surface was thereby assumed to be connected to a rigid motor.

The material for the housing was aluminum with a Young's modulus of $72 \cdot 10^3$ N/mm^2 and a density of $2.75 \cdot 10^{-9}$ tonnes/mm^3. The outer bearing rings was modeled using the same steel material used for the inner bearing rings. The total mass of the housing was $5.4096 \cdot 10^{-3}$ tonnes.

3.1.2 Eigenfrequency Analysis of Transmission Components

When reducing a finite element model into a substructure, a number of eigenmodes can be added in order to improve the dynamic representation of the substructure, see Section 2.7. To enable this, eigenfrequency analyzes of the individual components in Abaqus® were performed. Thereby the eigenfrequencies and their respective eigenmodes could be extracted and a number of eigenmodes could be included in the substructure. The method used for the mode addition to the substructure was the Craig-Bamptom method, see Section 2.7. Boundary conditions for the models had therefore to be introduced to fully constrain the models at the nodes which were to be retained during the substructuring process. The reason for the choice of using Craig-Bampton was that the interfaces between the different components had a relatively high stiffness. Alternatively the mixed-interface method could have been used, leaving for example the degrees of freedom associated with the rotation of the shafts unconstrained. However, as mentioned in Section 2.7, this could greatly increase the time consumption during the substructure generation process and the Craig-Bampton method was therefore preferred.

For the input shaft both of the bearing reference nodes, the spline reference node and the gear contact node were fixed in all degrees of freedom, i.e. nodes 50011, 50012, 101 and 1001 were completely fixed. Similar boundary conditions were applied for the main shaft, fixing the reference nodes of the bearings and the gear contacts in all degrees of freedom, i.e. nodes 50021, 50022, 2001 and 2002 were fixed.

The differential was also completely fixed at its bearing and gear contact reference nodes, i.e. nodes 50031, 50032 and 3002. The bevel gear shaft reference node in the middle of the differential was also fixed, i.e. node 301.

For each of the models, the first 20 eigenfrequencies and respective eigenmodes were evaluated. These are presented in Chapter 4.

3.1.3 Substructure Generation

After the frequency analysis step, the finite element models were reduced into substructures using the Craig-Bampton method, see Section 2.7. The retained degrees of freedom for the models were exclusively those involving contact and interaction with other components. All of the degrees of freedom associated to the nodes marked in Figure 3.2 to 3.6 were retained during the substructure generation, i.e. all of the reference nodes of the distributing and kinematic couplings. For each of the components, the extracted 20 first eigenmodes were also included in the substructures in order to improve the dynamic representation of the components.

After the substructure generation step, each component was reduced to a substructure, described by a mass matrix, a stiffness matrix and the generalized coordinates of the first 20 eigenmodes.

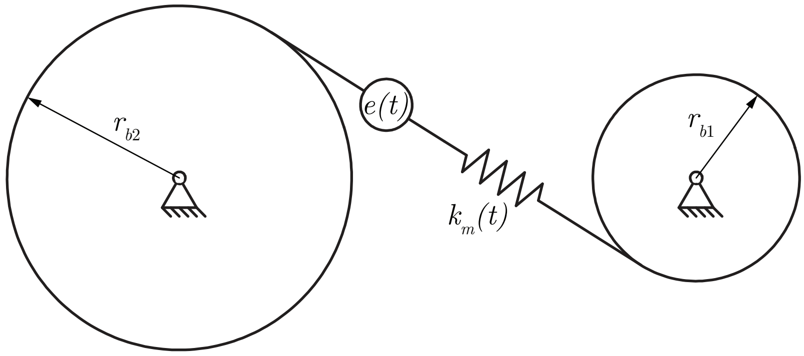

Figure 3.7: Illustration of the dynamical model used to describe the interaction in the gear contacts in the finite element model.

3.1.4 Gear Contact Modeling

For this thesis a dynamic model similar to the one proposed by Singh et al. [5] in 1990, see Section 2.6.1, was chosen to describe the interaction in the gear contacts. However, the effects of possible backlash and viscous damping were neglected in order to simplify the model. A representative illustration of the model used can be seen in Figure 3.7. The model basically consists of a time variant excitation and a time variant stiffness connected in series, connecting the two gears along the line of action. The transmission error for respective gear contact was used as excitation and the mesh stiffness for respective gear contact was used for the stiffness, as proposed by Singh et al. [5]. The transmission error therefore had to be expressed as a linear displacement along the line of action, according to Equation 2.14, in order to be adequate for the model.

The next step was to implement the theoretical model into Abaqus©, so that it could be used to connect the reference nodes in the gear contacts in the finite element model. The approach chosen was to use two so called connector elements available in Abaqus© to describe the behavior in the contact. These elements can be used in a number of applications, where complex connectivity behavior is involved. The element type used for the gear contact was the CONN3D2 element, which is a three-dimensional connector, connecting two nodes [21]. The relative motion of the connector elements must be specified, defining how the connector is acting. Behaviors can be assigned to the connector elements, e.g. elasticity and damping. Orientations of these behaviors can also be assigned to specify the direction of e.g. an elastic behavior. Also, prescribed motion of the connectors can be assigned as boundary conditions, allowing the elements to be used as displacement actuators.

The configuration of the two connectors used to represent the chosen model can be seen in Figure 3.8. One connector was elastic and the other was used as a displacement actuator. As described above, the reference nodes of the gear contacts were positioned at the pitch points of the gear pairs. The reference nodes of two gear contacts making a gear pair therefore coincide when the component models are assembled, which can be

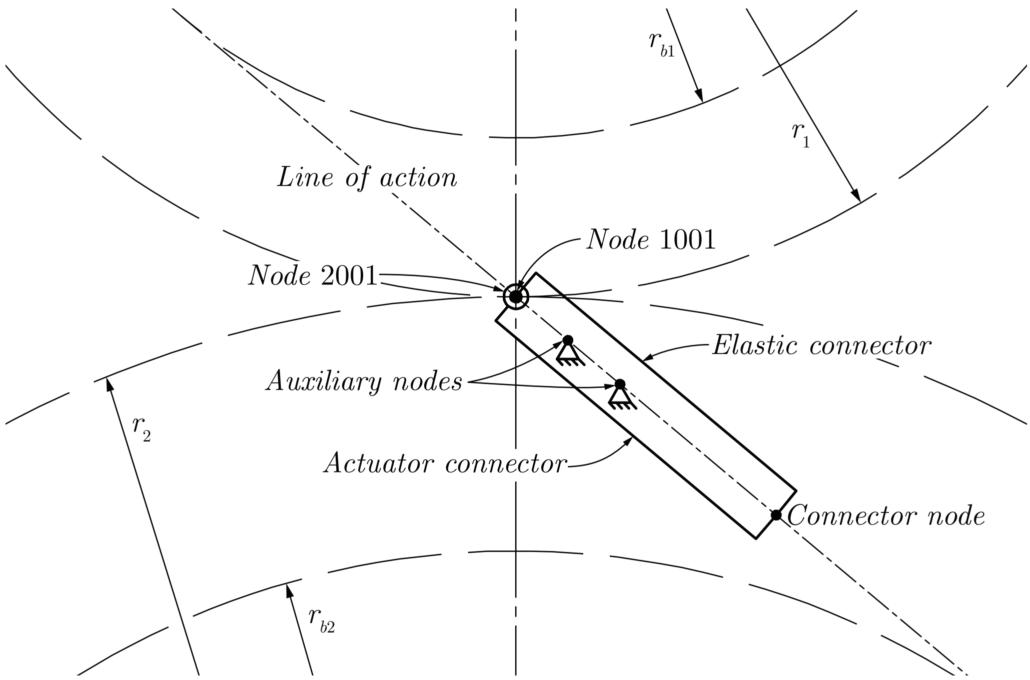

Figure 3.8: Illustration of the gear contact model as it was implemented in Abaqus®. The figure shows the gear contact between the input shaft and the main shaft, which can be seen in the numbering of the reference nodes, 1001 and 2001.

seen in the figure. The direction of the normal force in the gear contacts for each gear drive was known which enabled the introduction of two fixed auxiliary nodes to specify the direction of the line of action of the gear drive. One more node, called connector node in Figure 3.8, was introduced to connect the two connectors in series. The connector node was then constrained to slide along a line defined by the two auxiliary nodes, i.e. the line of action, thereby making the connectors aligned with the line of action. The two connectors were then given axial relative motion allowing them to act only along a line defined by the two nodes of each of the connectors.

In order to control the time dependent values for the displacement of the actuating connector and the elasticity of the elastic connector, an Abaqus© subroutine was created using Fortran©. The subroutine imported previously calculated values for the transmission error and the mesh stiffness for the examined loading conditions, see Section 3.3, and returned proper values to the connectors in the model for each time increment, see Section 3.4.2. The frequency of the excitation and the mesh stiffness variation depended on the rotational speed of the shafts. The transmission error was calculated over one mesh cycle, i.e. the cycle during which one gear teeth engages and disengages contact with the teeth of the meshing gear. The frequency with which each mesh cycle was repeated, f_m, was therefore obtained by multiplying the rotational speeds of the shafts with the number of gear teeth of the gear connected to respective shaft, z, according to

$$f_m = \frac{[\text{RPM of shaft}]}{60} \cdot z$$

The time period for one mesh cycle could then be obtained as

$$T_m = \frac{1}{f_m}$$

The subroutine used the mesh period of each gear contact to find the current position in the mesh cycle for any given point in time. This was achieved by dividing the current step time with the mesh period and thereby obtaining a remainder equivalent to the fraction of the current position in the mesh cycle. The data describing the transmission error and mesh stiffness were calculated at discrete positions in the mesh cycle, see Section 3.3, and interpolation was thus needed in order to obtain values for all possible mesh positions. Thereby, appropriate values for the displacements and stiffnesses of the connectors could be continuously imported to the simulation.

3.1.5 Bearing Modeling

The modeling of the bearings are of great importance when simulating the dynamic response in the housing of the transmission, since the vibrations caused by the variations in transmission error and mesh stiffness in the gear contacts are transferred through the bearings to the housing. To represent the behavior of each ball bearing, Vicura AB uses a specially designed bearing element. This element is based on an analytical model developed by L. Houpert in 1997 [23]. This model estimates the three bearing forces and the two tilting bearing moments as a function of the relative displacement and rotation (tilting) of the inner and outer bearing rings. This relationship is non-linear and the analytical model is implemented as an Abaqus® subroutine, previously developed by Vicura AB. The bearing element was used to connect the retained reference nodes of the outer bearing rings of the housing substructure to the retained reference nodes of the inner bearing rings of the shaft and differential substructures. For each incremental time step in the simulation, see Section 3.4.2, the bearing subroutine calculated and returned the stiffness matrix of the bearing element along with the reaction forces and moments acting in the element. Thereby, the behavior of each bearing could be described by a single element connecting two substructures.

3.2 Estimation of Transmission Loading

In order to obtain adequate values for the transmission error and the mesh stiffness of the gears in the transmission, reasonable loading conditions for the transmission was estimated. The examined transmission was designed for an electrical vehicle and thus designed to be driven by an electric motor. The exact motor model had not been specified, but according to the personnel at Vicura AB, a suitable motor would have a

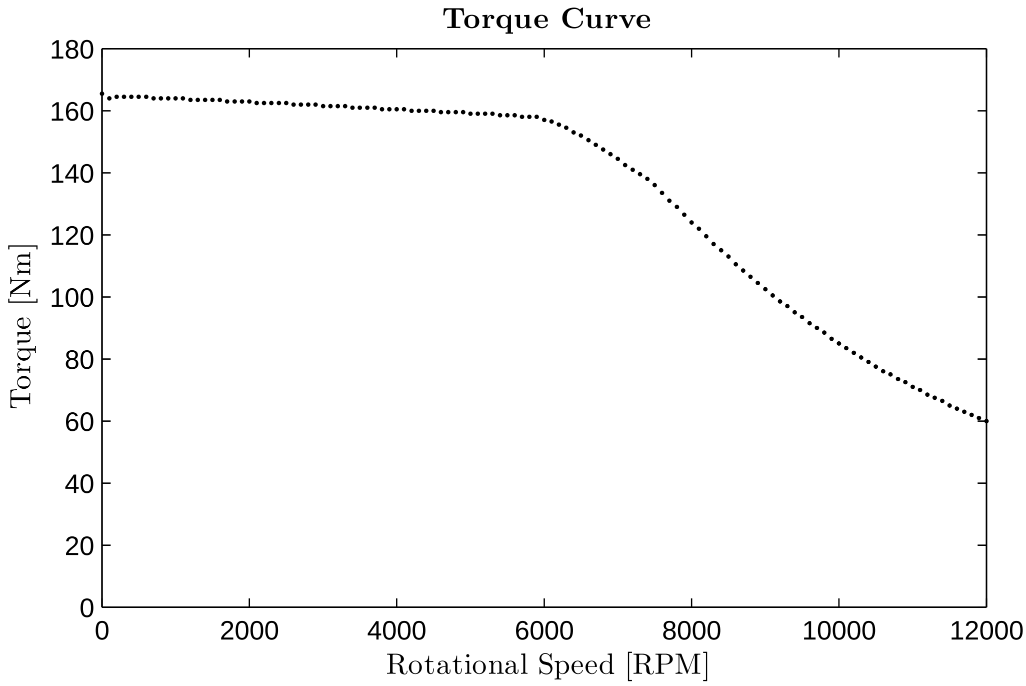

Figure 3.9: The relationship between maximum continuous torque and rotational speed of an electric motor suitable for the examined transmission.

maximum continuous torque-rotational speed relationship similar to the one illustrated in Figure 3.9. The motor can deliver a higher peak torque above these levels, but not for longer time periods. The reason for using the maximum torque is based on the hypothesis that a higher torque will result in a higher variation in the transmission error and thus result in more severe vibrations. It is therefore assumed to be a worst case loading condition for the transmission, with respect to gear whine noise. It can be seen that the motor delivers a relatively constant torque around 160 Nm for rotational speeds below 6,000 RPM. For higher rotational speeds the torque is decreasing with increasing rotational speed. The maximum rotational speed which can be delivered by the motor is approximately 12,000 RPM, with a torque of 60 Nm.

3.3 Calculation of Transmission Error and Mesh Stiffness

As input for gear contact subroutine used in the dynamic model, the time dependent transmission errors and mesh stiffnesses in the gear contacts had to be estimated. The calculations of the expected transmission errors and the mesh stiffness in the gear contacts of the transmission was performed using the Load Distribution Program© (LDP), developed by the Gear and Power Transmission Research Laboratory at The Ohio State University [24].

The LDP is a computer software tool for predicting the load distribution across the zone of contact for a single pair of spur or helical gears [24]. The model assumes that the load distribution is a function of the elasticity of the gears, including defined errors or modifications on the shape of the gear teeth. The total elastic deformation of the gear teeth is approximated as the sum of individual elastic deformations due to bending, shear and rigid deflection and rotation of the teeth. Also the deformation in the contact between the gear teeth is included. The deformations are based on analytical models, describing each of the different types of deformations. All of the elastic deformations are assumed to be small and thus tooth contact is assumed to remain on the line of contact [24]. The load distribution can then be estimated and a number of other factors can be obtained, such as the resulting transmission error, the mesh stiffness, stresses in root and gear contact, etc. For this work, the interesting output data was the transmission error and the mesh stiffness. The definition of transmission error in LDP follows Equation 2.14, i.e. as a linear displacement along the line of action. The main advantage of the LDP is that it allows for much faster calculations compared to e.g. finite element programs. As input for the LDP, a complete definition of a gear pair geometry and the torque loading must be provided in order for the analysis to be executable. The program then performs

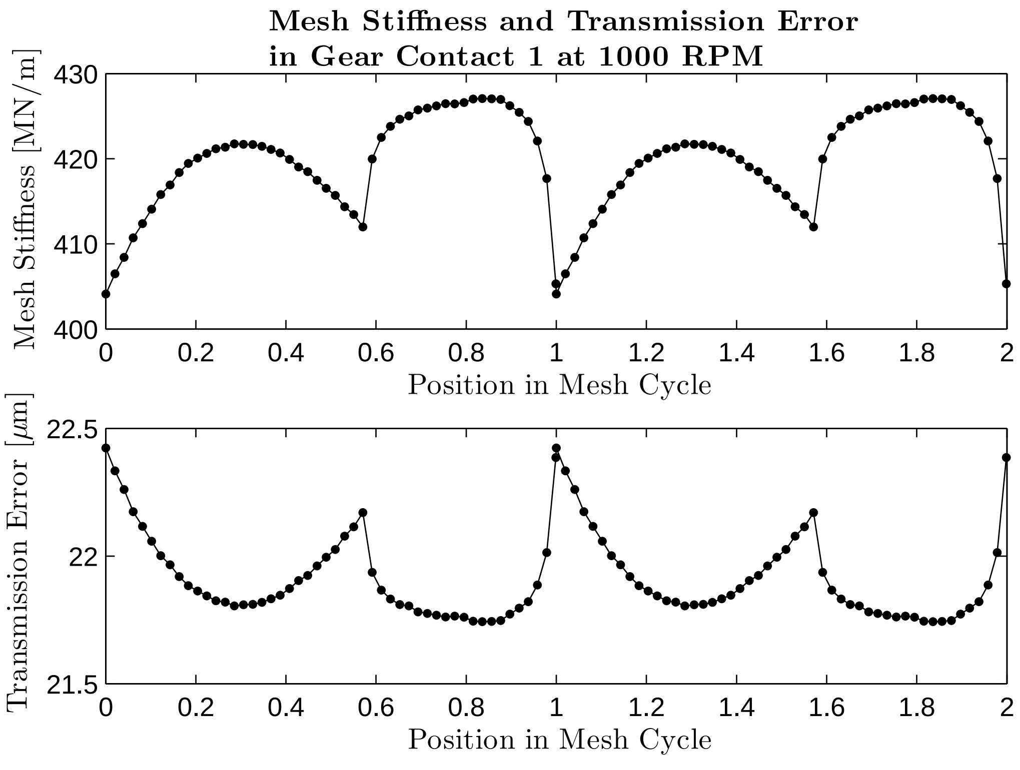

Figure 3.10: Examples of calculated mesh stiffness and transmission error using the LDP. It should be noted that the data in the figure is plotted over two mesh cycles.

static analyzes at a specified number of equally distributed positions through the mesh cycle of the gears at which data is obtained. Thereby data for e.g. the transmission error and the mesh stiffness through a full mesh cycle can be obtained. An example of a transmission error and a mesh stiffness curve can be seen in Figure 3.10.

Since the examined transmission includes two gear pairs, calculations for each individual gear pair were performed. Geometrical data, including micro-geometric modifications of the gear teeth, were specified as input in the LDP. The LDP can at this stage compute a theoretical contact ratio of the gear drive. This is the contact ratio if the gears are considered rigid. For the first gear contact the theoretical contact ratio was $CR_1 = 3.427$ and for the second gear contact the theoretical contact ratio was $CR_2 = 5.302$. This means that for the first gear contact the number of teeth in contact theoretically varies between three and four during a mesh cycle and for the second gear contact between five and six. From the example in Figure 3.10 for the first gear contact it can easily be seen when the number of teeth in contact changes from three to four at approximately 58% of the mesh cycle.

Mechanical calculations were then performed at intervals of 100 RPM, following the torque diagram described in Figure 3.9, at 50 discrete positions through the mesh cycle. Hence, a total number of 120 analyzes for each gear pair were conducted, in order to obtain values representing the full operating span of the motor, from 100 RPM to 12,000 RPM.

For the case of the input shaft to main shaft transfer, the torques from the motor were applied directly to the input shaft gear, using the values from the torque-RPM diagram. This was possible since there is no modification in the torque transferred from the shaft of the motor to the input shaft of the transmission since the shafts are directly connected. 120 different results were obtained, representing the different discrete operating conditions.

When evaluating the main shaft to the differential transfer, the torques applied on the main shaft had to be calculated. This is due to the gear ratio between the input shaft and the main shaft which changes the relation between the torques according to Equation 2.12. The torques for the main shaft were therefore obtained by multiplying the input shaft torques by the gear ratio of the two gears, i.e. $i_1 = 2.68$. As for the first gear pair, 120 different results were then obtained for the second gear pair.

The resulting transmission errors and mesh stiffnesses obtained from the LDP calculations were then manually exported to text files, one for each operating condition of the motor. For a range of rotational speeds of the motor the associated transmission error and mesh stiffness were thereby obtained. The results from the LDP calculations are presented and commented in Chapter 4.

3.4 Simulation Methodology

In order to evaluate the dynamic response of the transmission for the different load conditions, simulations were performed using the substructure models obtained in Section 3.1.3. All of the simulations were performed using the Abaqus® software and the solution process of each simulation consisted of three succeeding steps. The first and second were static steps used to initiate the bearing subroutine and to determine the displacements due to the applied torque. Thereafter a third, dynamic step was used to simulate the dynamic response of the system when excited by the transmission error and with a time varying mesh stiffness, in order to estimate the level of vibration of the reference nodes of the housing. Simulations were performed for rotational speeds from 100 RPM to 12,000 RPM at intervals of 100 RPM with respective input torques following the torque-rotational speed relationship described in Figure 3.9. The following sections will describe the boundary conditions and the solution procedure used for the simulations in greater detail.

3.4.1 Boundary Conditions

For the first step the transmission was fixed in space by assigning reference node 401 of the housing a zero displacement and rotation boundary condition. Due to the kinematic coupling between node 401 and the mounting surface of the transmission, this surface was thereby fixed. In order for a torque to be applied at the input shaft, the differential was prevented from rotating by assigning reference node 301 with a zero rotation condition in the rotational direction of the shafts. The degrees of freedom associated with the auxiliary nodes used for the gear contacts, see Section 3.1.4, were also fixed in order for the gear contact model to work as intended.

One problem with the bearing model was that it returned a zero stiffness matrix for the bearing elements if they were unloaded. Therefore, the reference nodes of the inner bearing rings (50011, 50012, 50021, 50022, 50031 and 50032 in Figures 3.2 to 3.5) were given initial translational displacements, while the reference nodes of the outer bearing rings (60011, 60012, 60021, 60022, 60031 and 60032 in Figure 3.6) were fully constrained. Thereby, the subroutine could iterate to obtain a proper bearing stiffness. The magnitude of the initial displacements were in the order of 10^{-2} mm, and the same values were used for all of the simulations.

The torque was then applied at the input shaft, by assigning a concentrated load to the reference node (101) at the spline coupling of the input shaft. The distributing coupling did then equally distribute the load to the splines. The load was assigned to the rotational degree of freedom in the rotational direction of the input shaft. This torque was then incrementally increased from zero to full loading during the simulation step in order to facilitate solution convergence. The magnitude of the torque depended on the drive condition simulated, following the torque-rotational speed relationship of the motor described in Figure 3.9.

Axial loads were also introduced, acting on the reference nodes of the gear contacts. The axial loads were calculated using Equation 2.11. For the gear contact between the input and main shaft, the input torque, base radius and helix angle of the gear attached to the input shaft were used to obtain the axial load using Equation 2.11. For the gear contact between the main shaft and the differential, the transferring torque first had to be calculated using Equation 2.12, given the gear ratio. The obtained axial loads were then applied to the gear contact reference nodes (1001, 2001, 2002 and 3002) in the axial directions, defined by the helix angles of the gears. As for the torque, the axial forces were applied gradually with each increment of the first simulation step, to finally reach their full magnitude in the last increment.

The connectors controlling the excitation in the gear contact model were fixed, while the mesh stiffnesses were given constant values for the first step equal to the average mesh stiffness for that input torque. It was thereby possible to obtain a static solution for the first step.

The second step had similar boundary conditions as the first step, with the difference that the reference nodes of the outer bearing rings were no longer fixed and the inner bearing rings did no longer have any prescribed displacement. The input torque and the axial loads were still applied at their full magnitudes and thereby the static deformation due to the applied input torque could be solved for.

For the third and final step in the simulations the connectors representing the excitation due to the transmission error and the time variant mesh stiffness were no longer fixed. Instead the gear contact model were assigned time dependent values for the excitation and the mesh stiffness using the amplitude subroutine. The subroutine imported the adequate transmission errors and mesh stiffnesses for the simulated loading condition, obtained in Section 3.3, and assigned them to the connectors in the contact model. The third step thereby made the simulation dynamic and time dependent. It should be noted that the shafts were not given any prescribed rotational velocity. Instead, the effects of the rotational speed was included by determining the mesh frequencies for the two gear drives, see Section 3.1.4.

3.4.2 Solver Procedure

All of the steps were solved using the Abaqus® implicit solver. For the first and second step in the simulation, static analysis was chosen and non-linear geometry was assumed. Linear geometry was evaluated but found inappropriate due to convergence problems. When performing non-linear analyzes in Abaqus®, each simulation step is divided into a number of so called time increments. For each time increment a number of iterations are required in order to find an equilibrium state [21]. In the context of static analyzes, time increments does not refer to actual physical time, but rather to a way to gradually increase loads and control convergence of the solution. For both the first and second step a total time of 1 s was used for each step. The solver was then controlled by setting a maximum and minimum value of the allowed time used for each increment. The solver then adjusted the length of the time increments depending on the number of iterations needed for each increment, within the defined limitations. If a time increment was too large and the solver needed too many iterations to solve the equations, the solver automatically reduced the length of the time increment and retried solving the equations. For both the first and second step a minimum time increment of $1 \cdot 10^{-5}$ s and a maximum time increment of 0.2 s was used in order to control the solution process.

The third and final step was a dynamic step used to evaluate the dynamic response of the system. Due to relatively small expected deformations, linear geometry was chosen for the third step. When performing a dynamic step in Abaqus® a step is divided into time increments as for the static case, but for the dynamic case the time increments represent physical time. As described above in Section 3.4.1 the third step involved time dependent boundary conditions which thereby were dependent on the size of the time increments.

The number of time increments and their size for the third step was decided from the following criterions. Firstly, enough time increments had to used for the simulations in order for the system to reach a steady-state response. After the system had reached a steady-state behavior, an appropriate number of samples at an appropriate sampling frequency had to be extracted in order to enable a FFT analysis of the response. For the FFT to work properly, the number of samples has to be of a power of two, see Section 2.8. A desired frequency spectrum up to $f_{\max} = 3{,}000$ Hz was chosen to be examined. The size of each time increment must therefore, according to the Nyquist criterion, be

$$\Delta t = \frac{1}{2f_{\max}} = \frac{1}{6{,}000}\,\mathrm{s} = 1.6667 \cdot 10^{-4}\,\mathrm{s}$$

The number of samples now dictates the resolution of the frequency spectrum obtained from a FFT analysis of the response, according to Equation 2.24. A high number of samples improves the resolution of the frequency spectrum but increases the computational time needed for each simulation. Test simulations were conducted in order to approximate a reasonable sample size and corresponding frequency resolution. It was established that a sample size of $n = 2{,}048$ samples would be reasonable. This was therefore used throughout the simulations and the resulting frequency resolution was according to Equation 2.24,

$$\Delta f = \frac{1}{n\Delta t} = \frac{1}{2{,}048 \cdot 1.6667 \cdot 10^{-4}}\,\mathrm{Hz} = 2.9297\,\mathrm{Hz}$$

Also, the time for the simulations to reach a nearly steady-state behavior was estimated to a corresponding 1,000 samples equivalent to 0.16667 s. For the third step a total of 3,048 time increments were then used, which resulted in a total time of the step to

$$T = n\Delta t = 3{,}048 \cdot 1.6667 \cdot 10^{-4}\,\mathrm{s} = 0.5080\,\mathrm{s}$$

As an attempt to shorten the time to reach a steady-state response, the excitations in the gear contacts were increased linearly from zero to full magnitude during the first 300 time increments in the third simulation step. The effect of this was however estimated to be minor, since the entire variation in the stiffness was still present.

3.5 Eigenfrequency Analysis of Simplified Transmission Model

There is no simple way of extracting the eigenfrequencies of the transmission model described above. This is due to the non-linear and time variant interactions existing between the different components, i.e. the gear contacts and the bearings. In order to obtain an estimation of the eigenfrequencies of the full model a simplified linear version of this model was developed. The elastic connectors in the gear contacts were given the average values of the mesh stiffnesses which amounted to $4.19446 \cdot 10^8$ N/m for the first gear contact and $7.60227 \cdot 10^8$ N/m for the second gear contact. This simplified the model so that no time variant mesh stiffnesses were considered. The actuating connectors were locked so that they became rigid elements without any variation in length and thus not exciting the system. The bearing elements were removed in the simplified model and the bearing reference nodes of the shafts and housing were instead pinned together, connecting the translations of the nodes but allowing free rotations. These simplifications are likely to increase the stiffness of the model.

The same static step used for the dynamic simulations described in Section 3.4 was used as an initial step in the extraction of the eigenfrequencies of the simplified transmission model. Thereafter followed a frequency extraction step same as for the individual transmission components in Section 3.1.2, extracting the 20 first eigenmodes. These are presented along with the results from the eigenfrequency analysis of the individual transmission components in Chapter 4.

3.6 Dynamic Response Analysis

In order to analyze the dynamic response of the transmission due to the transmission error excitation and the time dependent mesh stiffness, the displacements of the bearing reference nodes (60011, 60012, 60021, 60022, 60031 and 60032) of the housing were examined. The magnitude of the displacements and their respective point in time were extracted and exported to text files as time series. An example of such a time series can be seen in Figure 3.11, which shows the displacement of housing node 60032 during the third step of the simulation. The vertical line indicates the time point after the first 1,000 time increments of the third step had been completed. It can be seen that the solution for this case had not fully reached steady-state conditions during the proposed transient time period.

A common way to illustrate the dynamic response in a transmission is to use a so called waterfall plot. In a waterfall plot the magnitude of the displacements is plotted in a three dimensional diagram as a function of frequency and rotational speed [12]. In order to express the displacements for a specific rotational speed as a function of frequency instead of time, fast fourier transformation was used, see Section 2.8. This was implemented in a MATLAB® program, which first imported the displacement and time data for a node. The first 1,000 samples were then removed in order to obtain the last 2,048 samples. Note that 2,048 is an integer power of 2 ($2^{11} = 2{,}048$), which is necessary for the fast fourier transform to work. As can be seen from the example in Figure 3.11, the response varies around a static displacement of circa 0.1274 mm. It can also be seen that the static displacement is relatively large compared to the variations in the displacements. In the frequency domain, this constant component will therefore result in a high value at zero frequency, and will thus not provide any interesting information from a dynamic point of view. The static displacement was therefore removed by subtracting the average

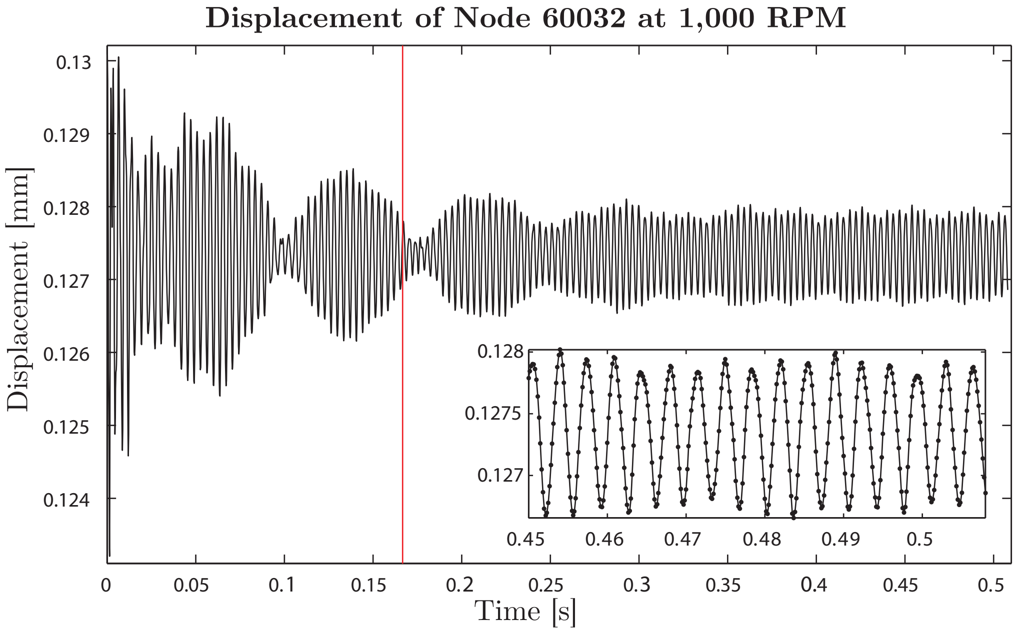

Figure 3.11: Example of dynamic response in reference node 60032 of the housing at 1,000 RPM. The vertical line indicates were the sampling period begins. A closeup of the last 346 samples is also included to illustrate the sample frequency.

displacement over the sampled period from each of the displacement samples. The program then performed a fast fourier transform using the function *fft* in MATLAB®, which implements Equation 2.22. The transformed data was then truncated in order to remove the complex conjugates, see Section 2.8, and a total number of $n/2 + 1 = 1{,}024$ values were obtained, each consisting of one real and one imaginary part. A frequency axis was then defined ranging from 0 to $(n/2)\Delta f \simeq 3{,}000$ Hz, at 1,024 equally spaced intervals of size $\Delta f = 2.9297$ Hz. By plotting the absolute values of the transformed data against the frequency axis, a frequency spectrum expressing the displacements as a function of frequency was obtained. The frequency spectrum corresponding to the displacement shown in Figure 3.11 calculated using the MATLAB® program can be seen in Figure 3.12.

By applying the program described above for every examined rotational speed, a waterfall plot could then be produced, which displayed the magnitude of dynamic response of the examined node as a function of both frequency and rotational speed. Since the housing had six reference nodes, six different waterfall plots were produced. These are presented and commented in Chapter 4.

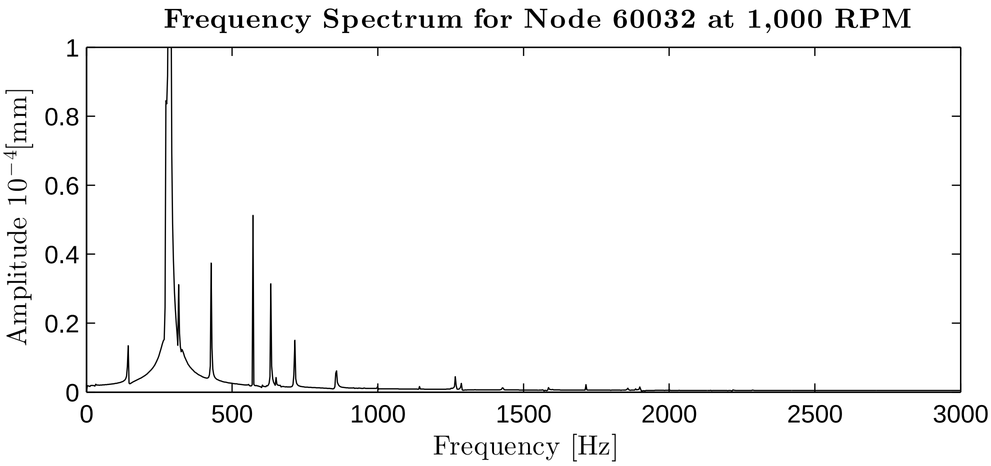

Figure 3.12: Frequency spectrum of the displacement curve in Figure 3.11, showing the amplitudes of the different frequency components of the curve.

4

Result

The results obtained from the different analyzes will be presented in this chapter. First of all, the resulting transmission errors and mesh stiffnesses for the two gear contact from the LDP analyzes is presented. Thereafter, the eigenfrequencies and the eigenmodes of the components included in the substructures for the dynamic simulations are presented. The dynamic response of the housing resulting from the dynamic simulations in Abaqus® is finally evaluated. The discussion of the results is found in Chapter 5.

4.1 Transmission Errors and Mesh Stiffnesses in Gear Contacts

This section presents the results obtained from the LDP analyzes described in Section 3.3. The interesting results from the analyzes in this context are the transmission errors and the mesh stiffnesses for each of the loading conditions shown in the diagram in Figure 3.9. These results have been used as time variant input for the gear contact used in the dynamic simulations.

4.1.1 Calculated Transmission Error

The transmission error in the first gear contact is plotted for each of the loading conditions in Figure 4.1. It should be noted that the rotational speed is not included in the LDP analyzes. Instead, the torque associated to the rotational speed following the diagram in Figure 3.9 is the variational factor. It can be seen that the magnitude of the transmission error is greatest for rotational speeds below 6,000 RPM, corresponding to torques between 165.5 Nm and 158 Nm. As the rotational speed increases above this level, the transmission error decreases in magnitude. The transmission error in the first gear contact ranges between a minimum of 10.21 μm to a maximum of 22.48 μm.

From a dynamic point of view, it is the variation in the transmission error over the

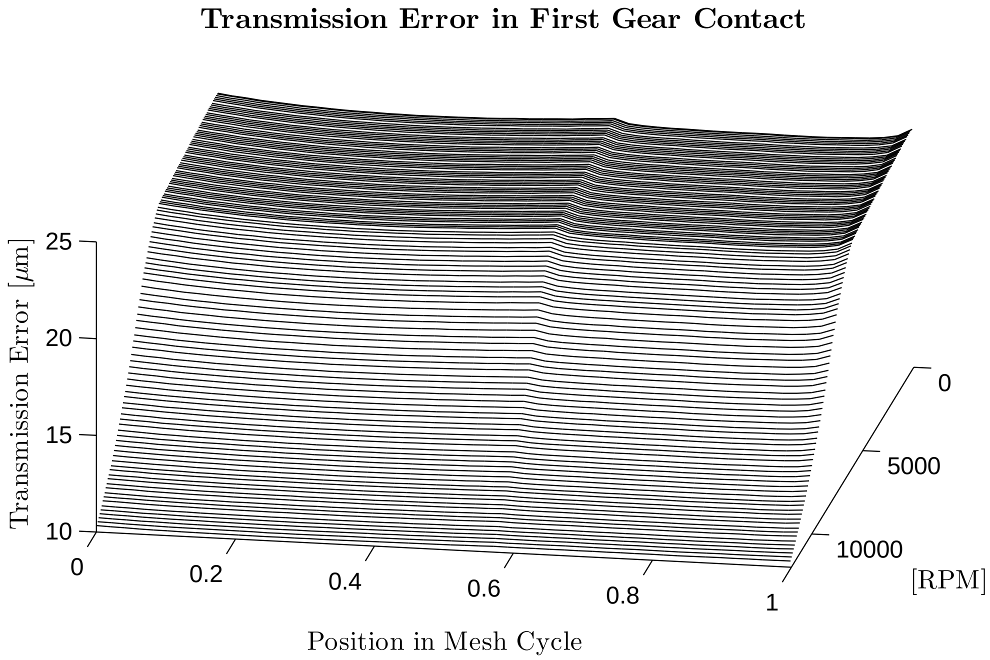

Figure 4.1: Transmission error for the first gear contact.

mesh cycle which is of greater importance, rather than the absolute transmission error. Figure 4.2 shows the variational part of the transmission error in the first gear contact plotted for each of the examined loading conditions. The variational part was obtained by subtracting the average transmission error for each loading condition. It can be seen that the variation in the transmission error is highest for the lower rotational speeds, corresponding to higher torques. The highest peak-to-peak transmission error amounts to 0.683 μm and the lowest amounts to 0.122 μm.

The results for the transmission error in the second gear contact can be seen in Figure 4.3. It can be seen that a the transmission error follows a similar pattern as for the first gear contact, i.e. relatively constant from 100 to 6,000 RPM after which it is decreasing for increasing rotational speed. The overall magnitude is however larger, ranging from a minimum of 16.49 μm to a maximum of 31.07 μm. It should be noted that the torques used for the calculation of the transmission error in the second gear contact are higher compared to the first gear contact, due to the gear ratio between the input shaft and the main shaft, as stated in Section 3.3.

The variational part of the transmission error in the second gear contact can be seen in Figure 4.4 and it was obtained using the same procedure as for the first gear contact. It can be seen that the variation is highest for the lower rotational speeds, with a maximum peak-to-peak transmission error of 0.346 μm and a minimum of 0.106 μm. Even though the total transmission error in the second gear contact is generally higher than that for the first gear contact, the variation in transmission error is generally lower.

Variation in Transmission Error in First Gear Contact

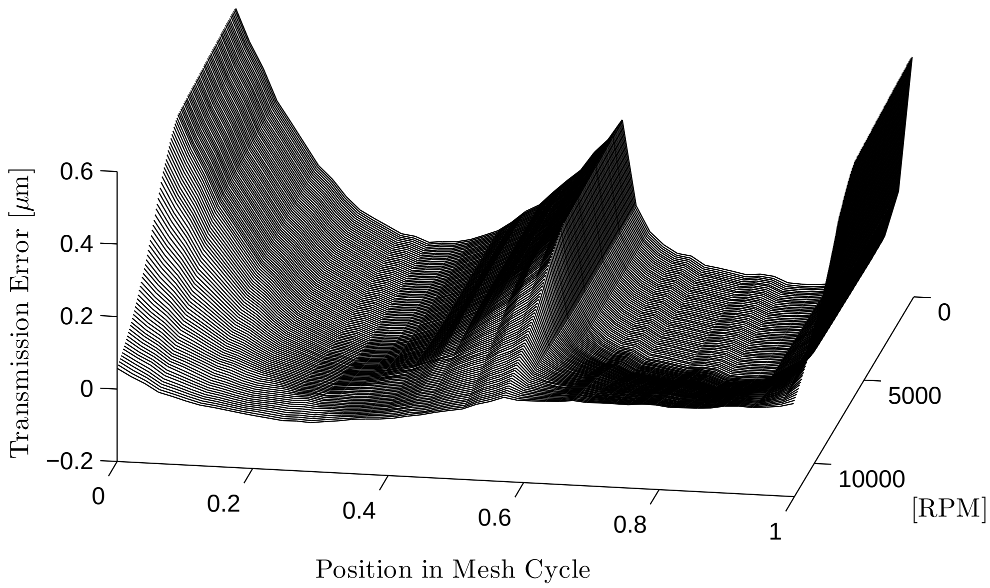

Figure 4.2: Variational part of the transmission error for the first gear contact.

Transmission Error in Second Gear Contact

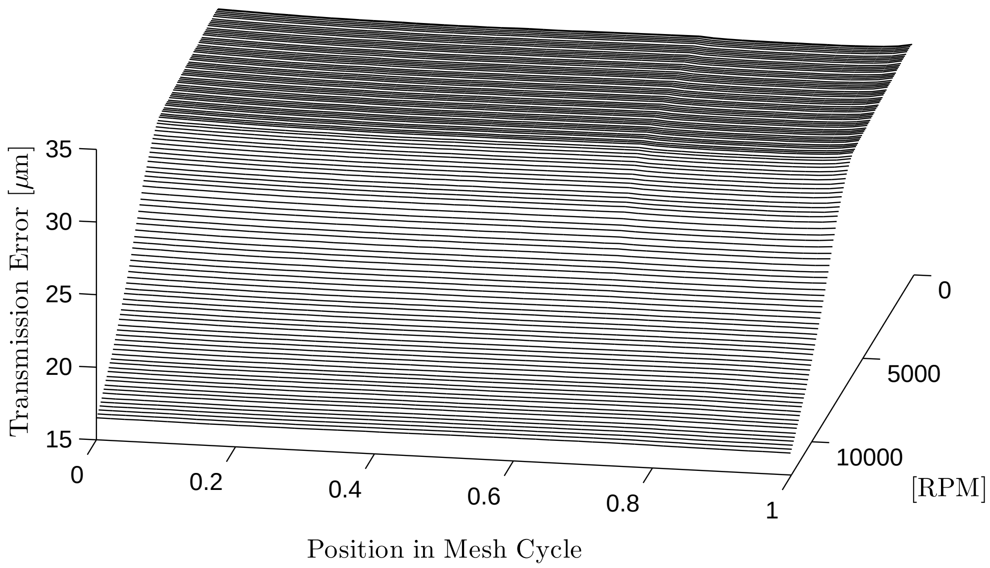

Figure 4.3: Transmission error for the second gear contact.

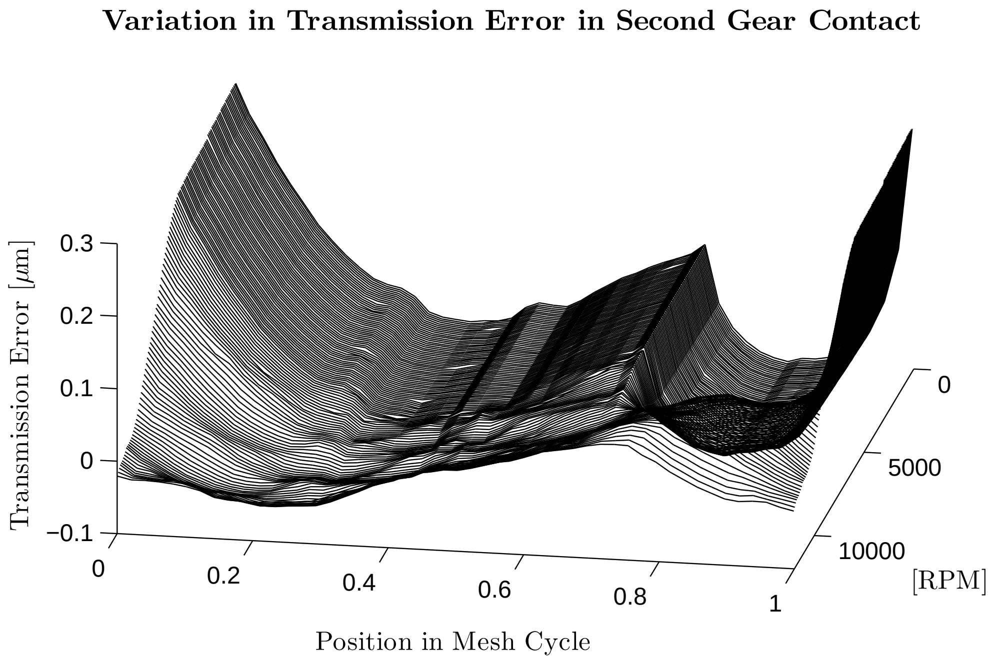

Figure 4.4: Variational part of the transmission error for the second gear contact.

4.1.2 Calculated Mesh Stiffness

The mesh stiffness in the first gear contact can be seen in Figure 4.5. It can be seen that the mesh stiffness decreases with increasing rotational speed, and thus decreasing torque. The maximum mesh stiffness in the first gear contact amounts to $4.27 \cdot 10^8$ N/m and the minimum mesh stiffness amounts to $3.76 \cdot 10^8$ N/m.

As for the transmission error, the variation in mesh stiffness can be examined. Figure 4.6 shows the resulting variation in mesh stiffness for the loading cases. It can be seen that the variation is relatively unchanged for the different rotational speeds. However, a small increase in the variation can be seen as the rotational speed reaches above circa 6,000 RPM. The peak-to-peak mesh stiffness in the first gear contact range between a minimum of $2.26 \cdot 10^7$ N/m and a maximum of $2.47 \cdot 10^7$ N/m.

The mesh stiffness in the second gear contact can be seen in Figure 4.7. A similar pattern as for the first gear contact can be seen, except at the higher rotational speeds, where there is a change in the overall relationship of the stiffness. The magnitudes of the mesh stiffness in the second gear contact range from a minimum of $5.58 \cdot 10^8$ N/m to a maximum of $7.73 \cdot 10^8$ N/m. It can be seen that the mesh stiffness is significantly higher in the second gear contact as compared to the first gear contact.

The variation in the mesh stiffness in the second gear contact can be seen in Fig-

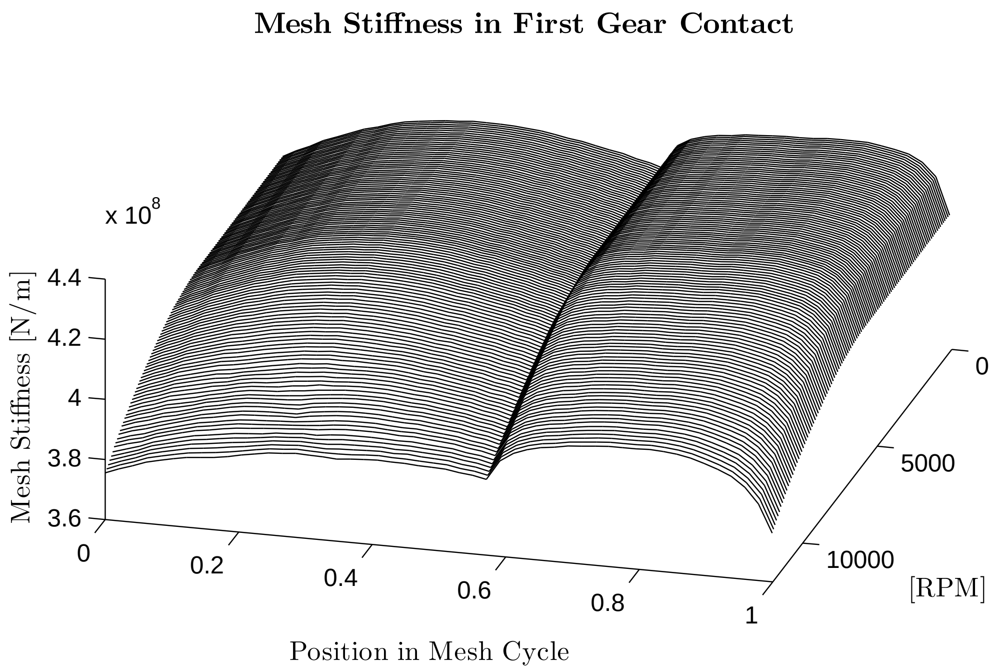

Figure 4.5: The calculated mesh stiffness in the first gear contact.

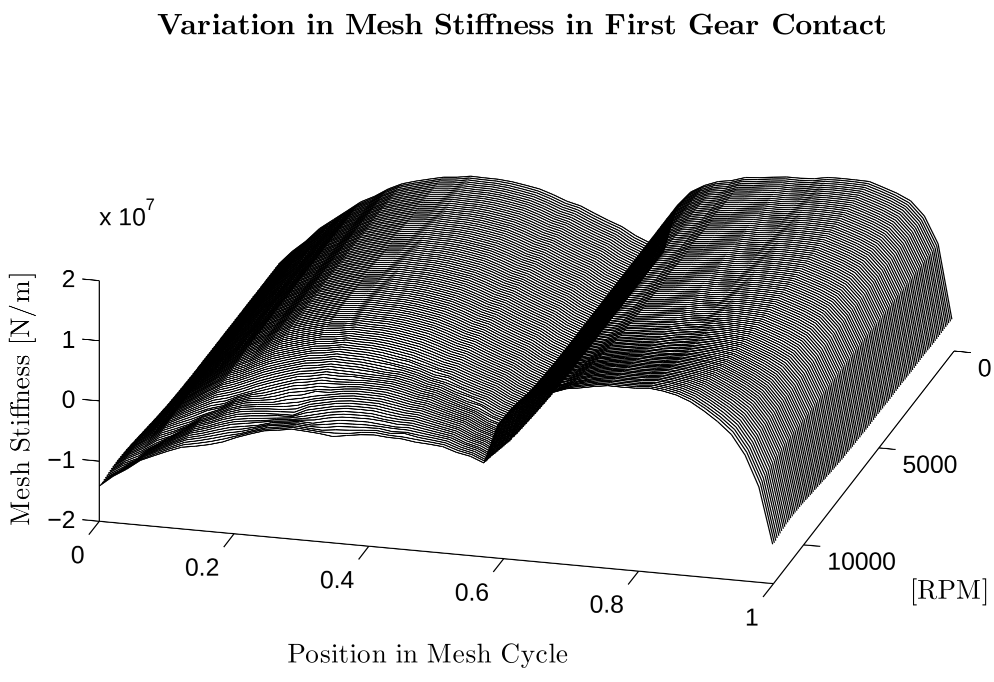

Figure 4.6: Variational part of the mesh stiffness in the first gear contact.

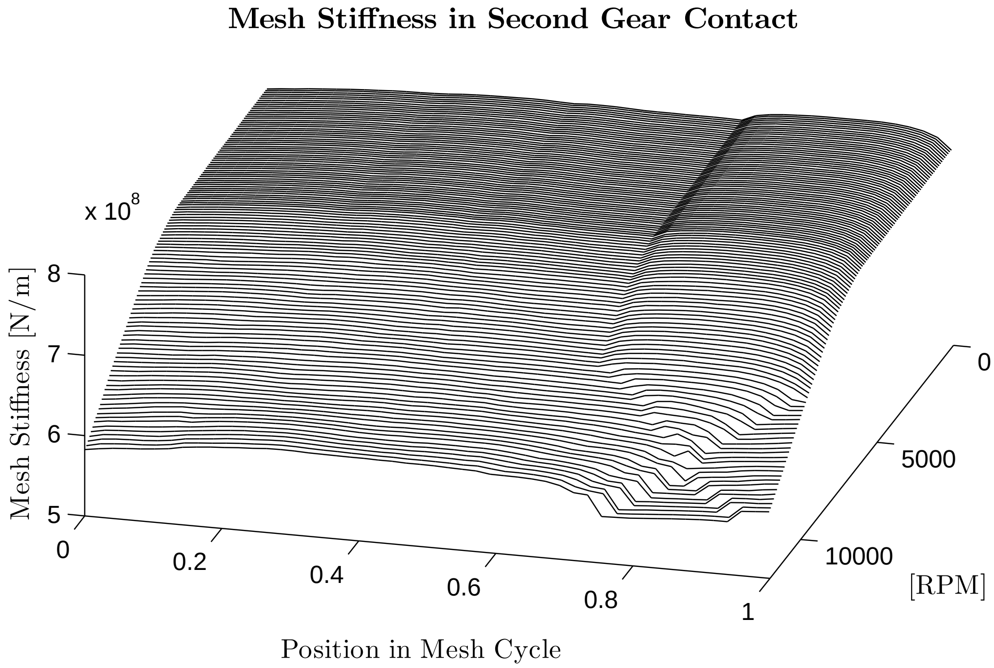

Figure 4.7: The calculated mesh stiffness in the second gear contact.

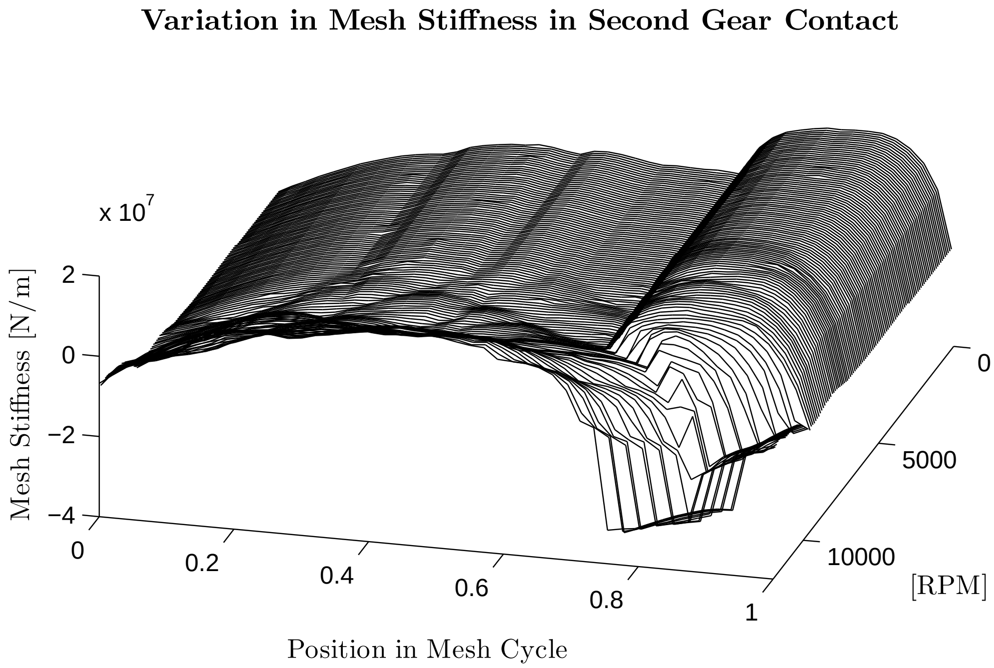

Figure 4.8: Variational part of the mesh stiffness in the second gear contact.

ure 4.8. The variation remains relatively unchanged until the rotational speed reaches circa 9,000 RPM, corresponding to a torque of 102.5 Nm. At that level, the mesh stiffness exhibits a great transit in variation. The variation over the mesh cycle changes completely and generally increases in magnitude. This is due to a change in the contact ratio of the gear contact. It changes from alternating between five and six gear teeth in contact to alternating between five and four for the lower loadings. This behavior is caused by the modifications of the so called micro geometry of the gears. These are modifications of the gear teeth which are used to compensate for the deformations in the gear teeth when the gears are loaded. A small comparison using zero modifications for the second gear contact, i.e. using the theoretical gear profile shape described in Section 2.2, resulted in a more uniform behavior in both the transmission error and the mesh stiffness. The peak-to-peak transmission errors were however instead increased by a large factor (maximum 0.881 μm, minimum 0.318 μm). For the lower torque loadings, the micro geometry of the gear teeth in the second gear contact is overcompensating for the deformations and instead resulting in the transit in the overall behavior of the mesh stiffness. The maximum peak-to-peak value for the mesh stiffness in the second gear contact amounts to $0.474 \cdot 10^8$ N/m while the minimum peak-to-peak value amounts to $0.238 \cdot 10^8$ N/m.

4.2 Eigenfrequency Analyzes

The calculated eigenfrequencies of the transmission components are presented in Table 4.1 along with the eigenfrequencies of the simplified transmission model. It should be noted that the eigenfrequencies for the components correspond to when the reference nodes of the bearings are fully constrained in all six degrees of freedom. The first four eigenmodes for each of the transmission components are also visualized in Figures 4.9 to 4.12. It is these along with the next 16 eigenmodes of the components which have been included in the substructures used in the simulations. The eigenmodes of the simplified transmission are difficult to illustrate since they only involve the retained nodes of the components. It can however be noted that the lowest eigenmodes involve large deformation at the connection point between the differential and the housing.

Table 4.1: Calculated eigenfrequencies for the components of the transmission and the simplified transmission model.

Eigen - frequency	**Input Shaft [Hz]**	**Main Shaft [Hz]**	**Differential [Hz]**	**Housing [Hz]**	**Transmission [Hz]**
1	14278	2913	2502	2114	311
2	14297	3145	2761	2517	360
3	16400	3628	2926	3242	616
4	17584	4281	3608	3392	743
5	19782	4333	3767	3915	955

6	19868	4364	4749	4243	1164
7	22073	4403	5209	4294	1325
8	22764	4779	5654	4818	1736
9	22965	5088	6098	4920	1864
10	23762	5893	6537	5016	1975
11	25545	6530	7117	5250	2024
12	26192	7007	7212	5569	2145
13	27378	7657	7411	5676	2331
14	28242	8453	8019	5902	2425
15	31549	8554	8408	6032	2461
16	31611	8768	8469	6176	2627
17	32043	8887	9743	6294	2890
18	32079	10929	9899	6460	3015
19	32854	12141	10234	6734	3081
20	33484	12441	10431	6832	3155

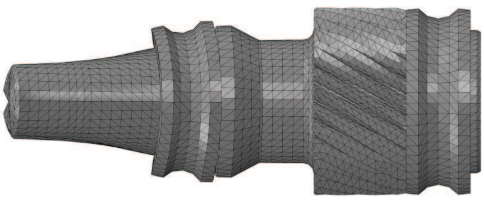

Mode 1 - 14,278 Hz

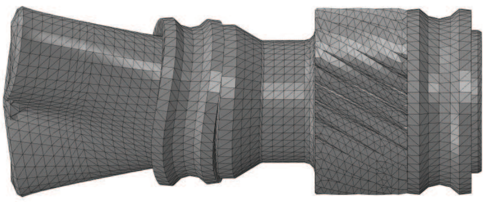

Mode 2 - 14,297 Hz

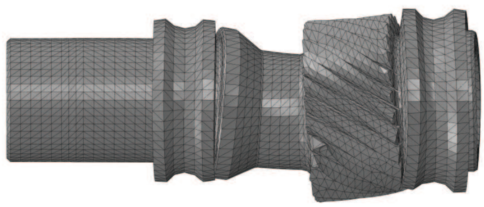

Mode 3 - 16,400 Hz

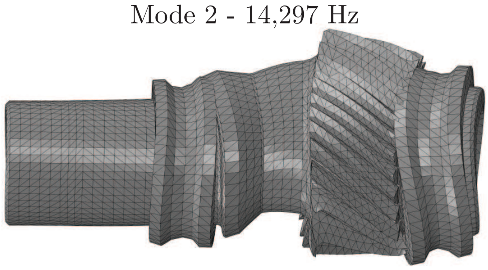

Mode 4 - 17,584 Hz

Figure 4.9: The first four eigenfrequencies and corresponding eigenmodes of the input shaft (displacements not to scale).

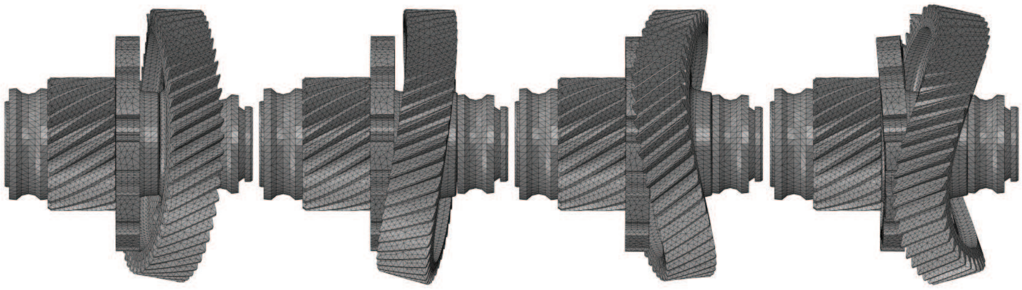

Mode 1 - 2,913 Hz Mode 2 - 3,145 Hz Mode 3 - 3,628 Hz Mode 4 - 4,281 Hz

Figure 4.10: The first four eigenfrequencies and corresponding eigenmodes of the main shaft (displacements not to scale).

Mode 1 - 2,502 Hz Mode 2 - 2,761 Hz Mode 3 - 2,926 Hz Mode 4 - 3,608 Hz

Figure 4.11: The first four eigenfrequencies and corresponding eigenmodes of the differential (displacements not to scale).

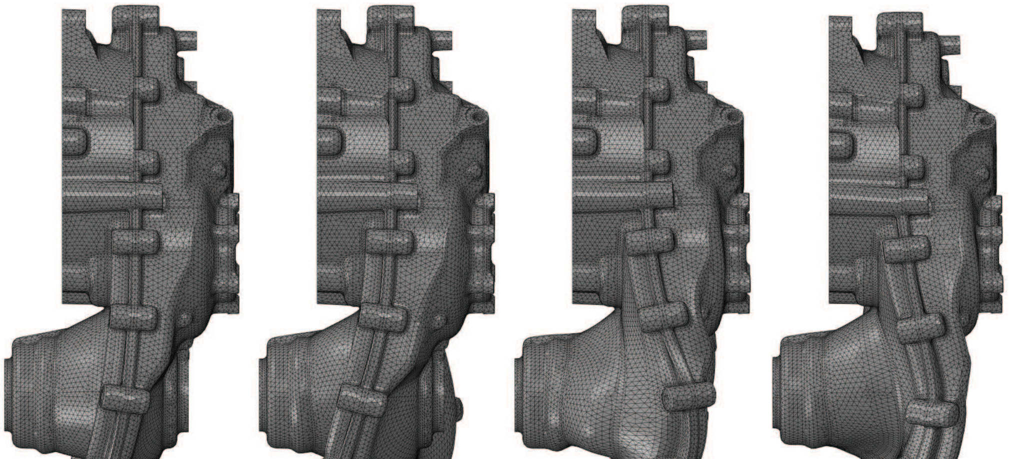

Mode 1 - 2,114 Hz Mode 2 - 2,517 Hz Mode 3 - 3,242 Hz Mode 4 - 3,392 Hz

Figure 4.12: The first four eigenfrequencies and corresponding eigenmodes of the housing (displacements not to scale).

From Table 4.1 it can be seen that the first eigenfrequencies for the components are 14,278 Hz, 2,913 Hz, 2,502 Hz and 2,114 Hz for the input shaft, main shaft, differential and the housing respectively. The eigenfrequencies of the input shaft are considerably higher compared to the other components. The mass of the input shaft model is only 0.9599 kg compared to e.g. the main shaft with a mass of 2.666 kg. This low mass in combination with a relatively stiff and highly constrained geometry is the reason for the high eigenfrequencies of the input shaft.

The eigenfrequencies for the simplified transmission model are overall much lower compared to the components. This is due to the greater mass contra stiffness of the entire transmission along with the less constrained boundary conditions, which reduces the eigenfrequencies.

4.3 Dynamic Response of the Transmission Housing

The dynamic response of the housing reference nodes (seen in Figure 3.6) due to the excitations in the gear contacts was investigated in order to map the dynamic behavior of the transmission for the different loading conditions. Thereby the expected levels of vibrations which the housing could be exposed to can be estimated.

For each of the 120 examined loading conditions, the displacements of the bearing reference nodes of the housing for each time increment were obtained from the simulations described in Section 3.4. For the case of 3,000 RPM, 6,000 RPM and 9,000 RPM, the displacements of the mentioned nodes are plotted against time in Figures 4.13 to 4.15. It should be noted that the time span in the plots is the time period used as sampling period of the data from the simulations and corresponds to a total of 2,048 samples for each node. It can be seen that the overall static deformation of the housing is largest at nodes 60031 and 60032, where the differential is connected to the housing. The variations in the displacements caused by the excitations in the gear contacts are small compared to the overall static deformations, typically in the magnitude order of 10^{-1} μm. The nodes 60011, 60012 and 60022 have all reached relatively converged steady-state conditions before the beginning of the sampled period. The other examined nodes exhibit a transient behavior during the sampled period, especially nodes 60031 and 60032. These nodes do however reach a steady-state behavior after approximately half of the sampled time period. The average total time consumption for each of the 120 simulations was circa 4,900 s ($\sim$ 1h 22 min) when computed using a 3.47 GHz CPU.

Waterfall plots showing the frequency components of the resulting displacements of the housing bearing reference nodes for all of the examined loading conditions were obtained using the fast fourier transform methodology described in Section 3.6. These are plotted for each housing node in Figures 4.16 to 4.21.

Generally it can be seen that for all of the reference nodes, amplitude peaks which gradually shift from lower to higher frequencies as the rotational speed is increasing appear in the waterfall plots. These peaks correspond to the harmonics of the two mesh frequencies, which determined the frequencies with which the mesh cycles were repeated in the gear contact subroutine, see Section 3.1.4. The most distinct harmonic for all

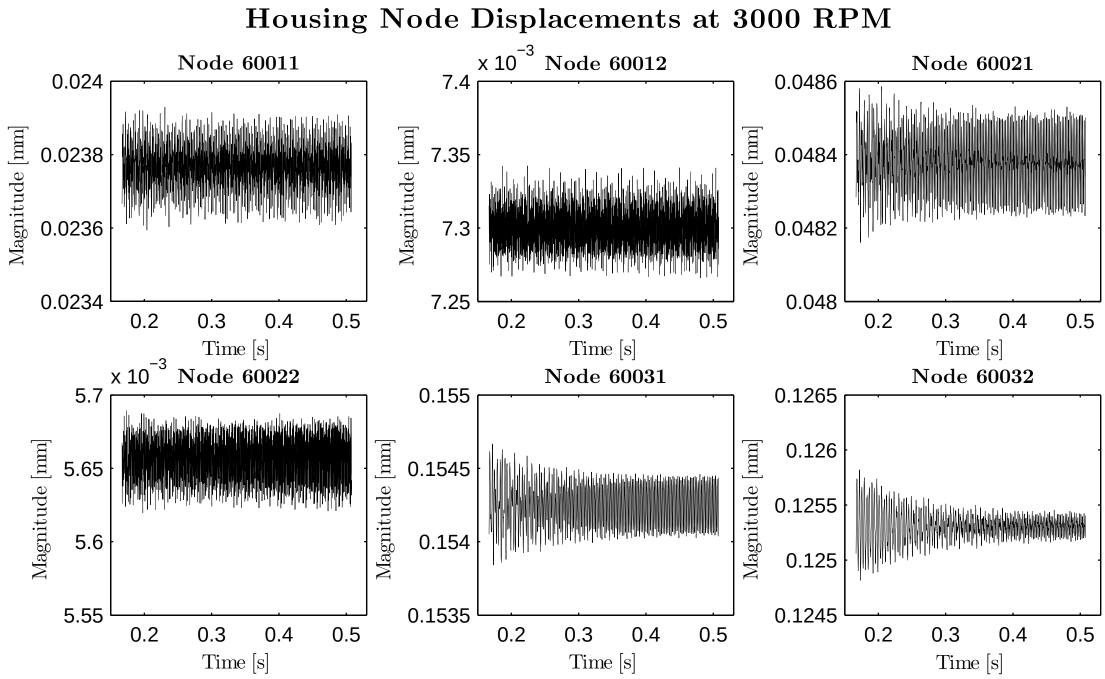

Figure 4.13: Time-displacement graphs of the housing nodes at 3,000 RPM.

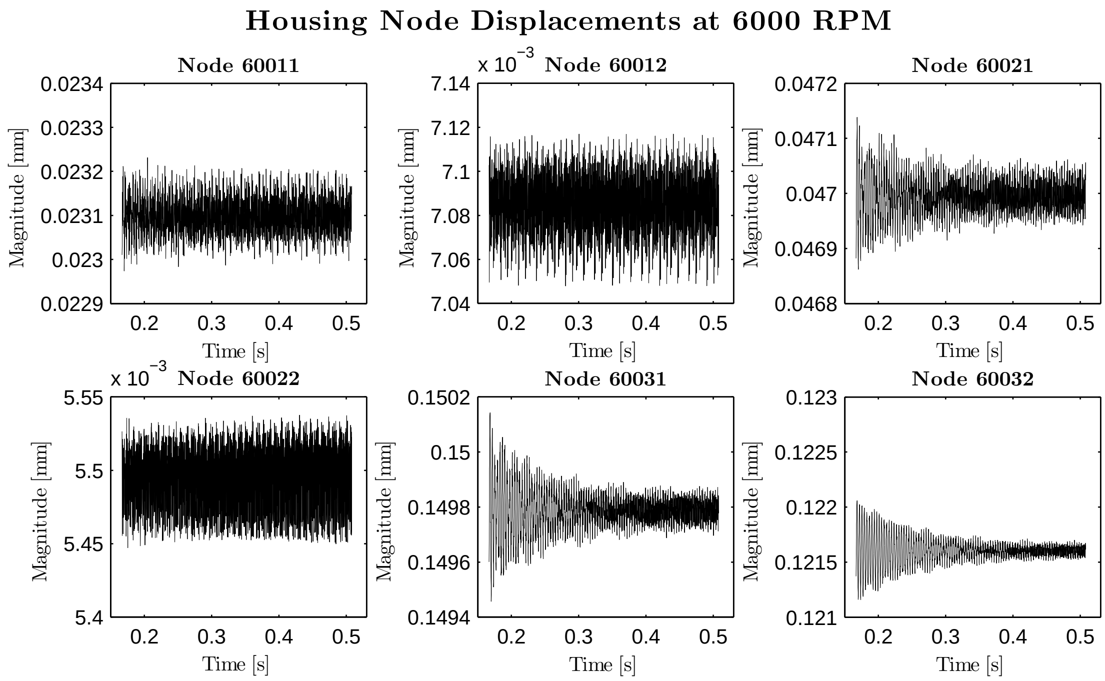

Figure 4.14: Time-displacement graphs of the housing nodes at 6,000 RPM.

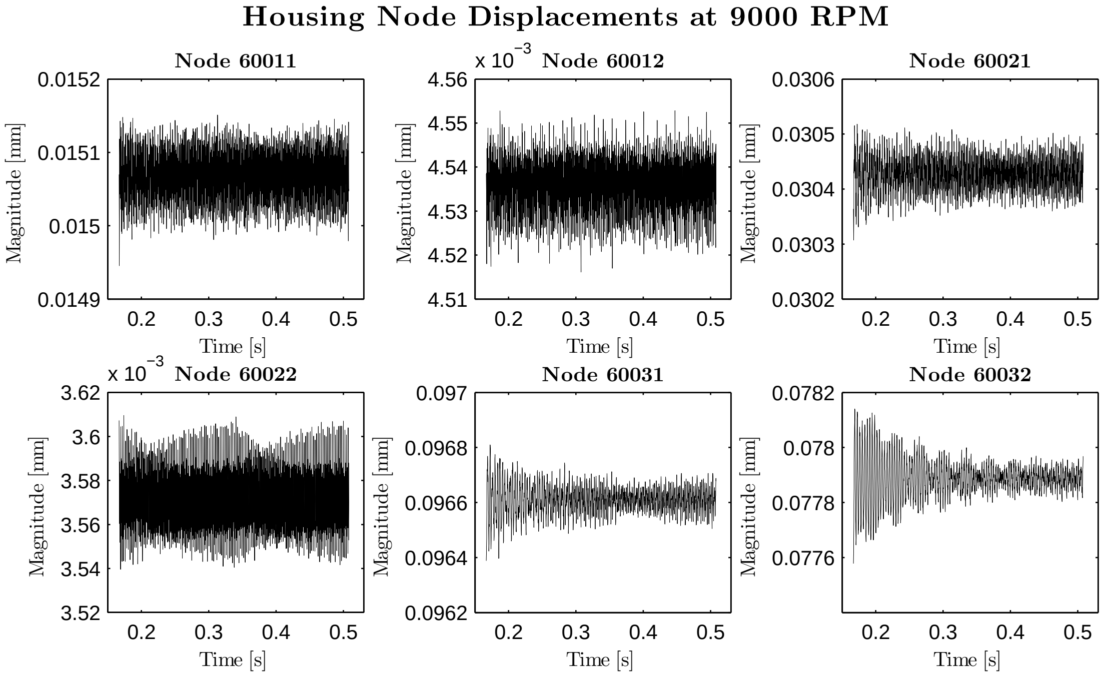

Figure 4.15: Time-displacement graphs of the housing nodes at 9,000 RPM.

examined nodes is the one corresponding to the first harmonic of the mesh frequency in the second gear contact. This can be seen clearly in Figure 4.17, where some of the harmonics are marked. Thereafter follows the second harmonic of the second gear contact closely followed by the first harmonic of the first gear contact. The third and and forth harmonics of the second gear contact can also be identified in the plots as the following two ridges in the waterfall plots.

Another interesting observation is the amplitude peaks which appear at the same frequency components, regardless of the rotational speed of the input shaft. This occurs at three rather distinct frequencies, at circa 273 Hz, 340 Hz and 550 Hz. If these frequencies are compared to the obtained eigenfrequencies from the simplified transmission model presented in Table 4.1, it can be seen that they correspond to the first three eigenfrequencies of the transmission. They appear at slightly lower frequencies than those evaluated for the simplified model due to its simplifications which increased the stiffness of the model and thus resulting in slightly higher eigenfrequencies.

It can be seen for all nodes that when the mesh frequencies coincide with the eigenfrequencies, significant amplitude peaks appear caused by resonance in the system. The highest amplitude is observed for node 60032 in Figure 4.21 where the first harmonic of the second gear contact mesh frequency coincide with the first eigenfrequency of the system. Generally, for all of the examined nodes, elevated amplitude peaks appear for the frequency components in the range between 1,000 to 2,000 Hz.

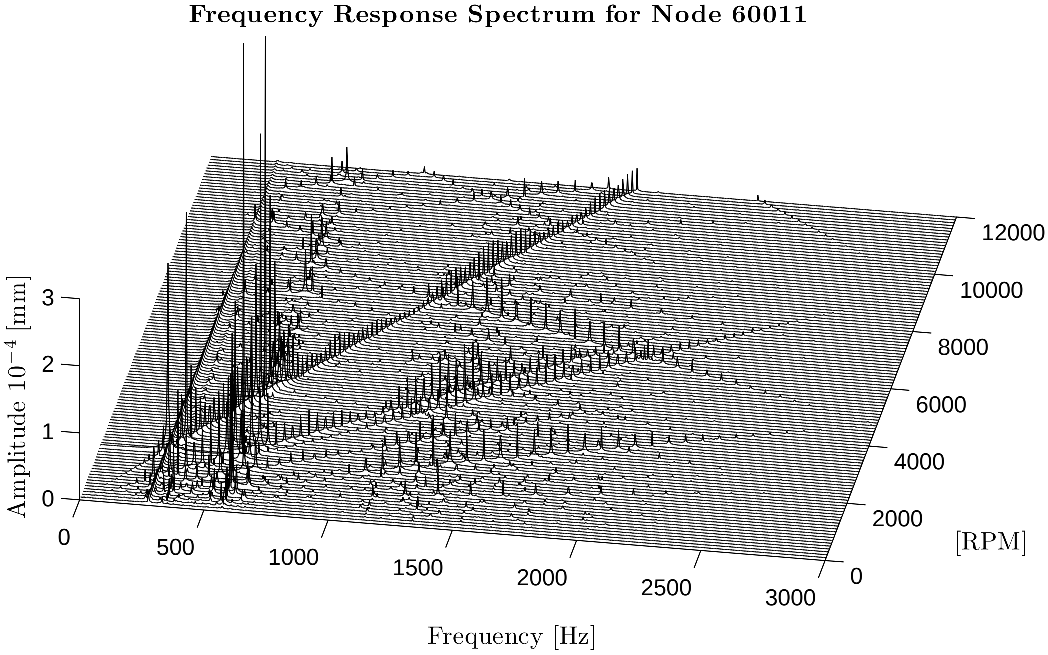

Figure 4.16: Waterfall plot displaying the dynamic response of reference node 60011.

Amplitude peaks which gradually shift from higher to lower frequencies can be observed at rotational speeds above circa 5,000 RPM. This is likely to be caused by aliasing, see Section 2.8. When the harmonics of the mesh frequencies reach frequencies above the Nyquist frequency, in this case 3,000 Hz, they appear at lower frequencies when the fast fourier transform is performed. According to [3], frequencies above the Nyquist are reflected about the Nyquist frequency, which would explain the amplitudes shifting from higher to lower frequencies for increasing rotational speeds in the waterfall plots. The reflected amplitudes should therefore not be considered to any greater extent, since they appear at wrong frequency intervals in the waterfall plots.

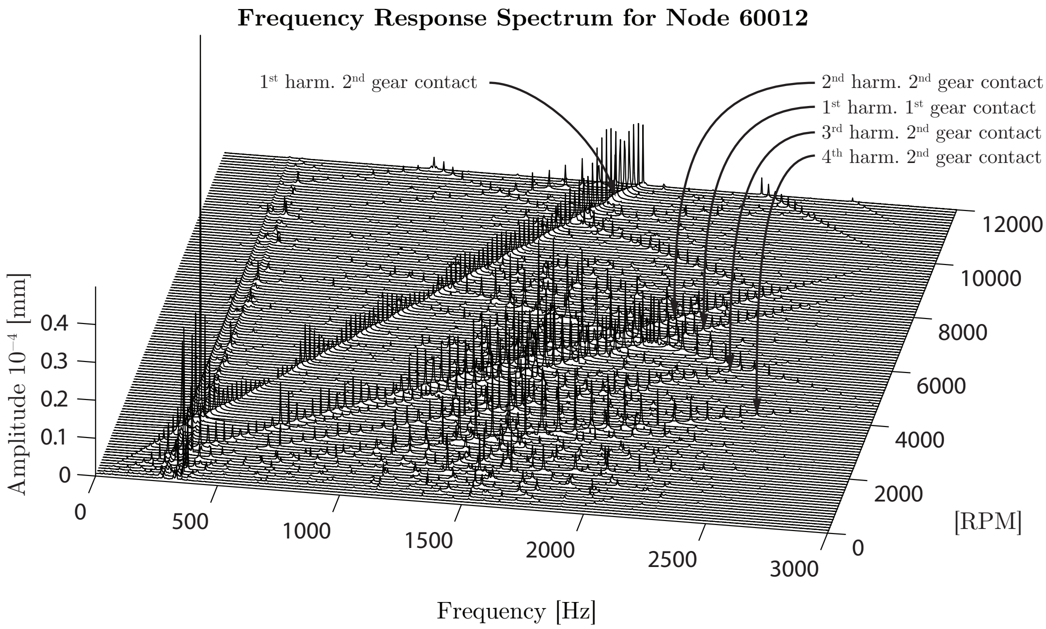

Figure 4.17: Waterfall plot displaying the dynamic response of reference node 60012.

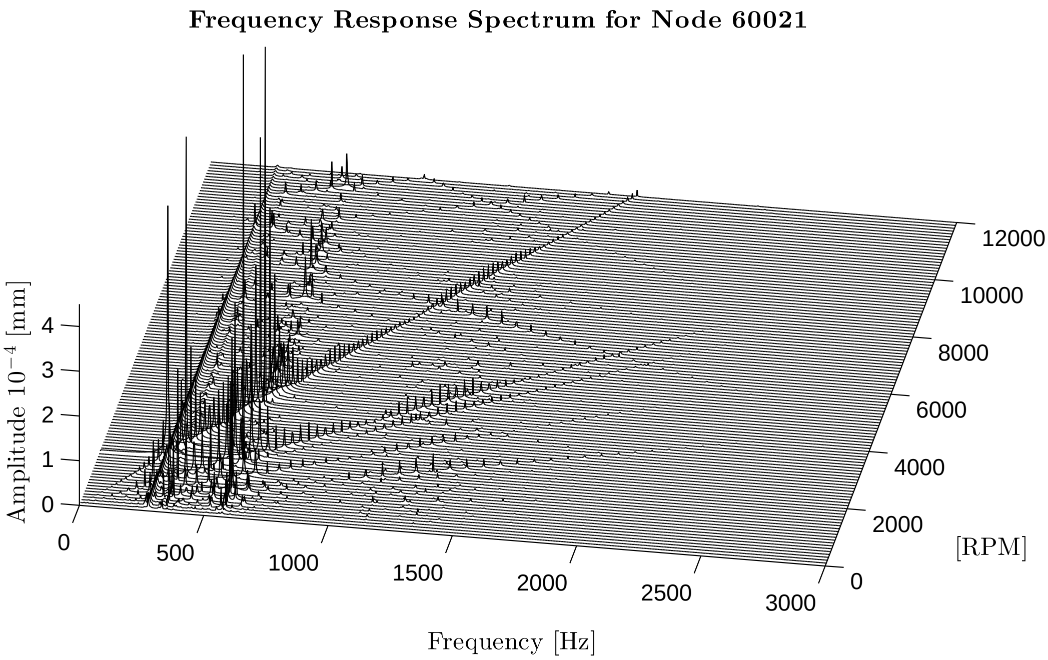

Figure 4.18: Waterfall plot displaying the dynamic response of reference node 60021.

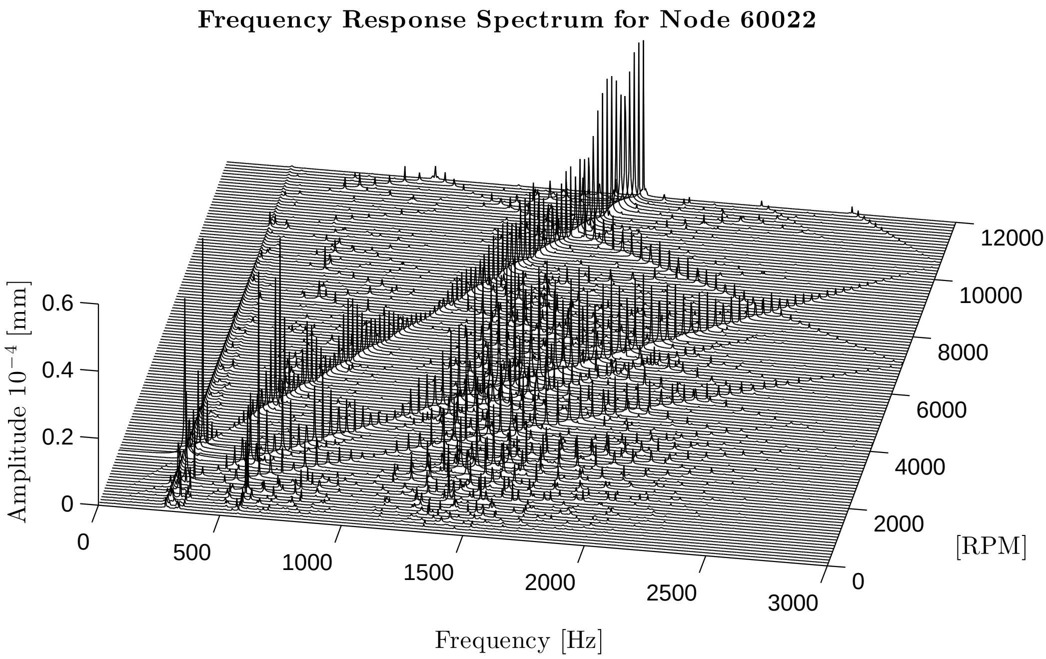

Figure 4.19: Waterfall plot displaying the dynamic response of reference node 60022.

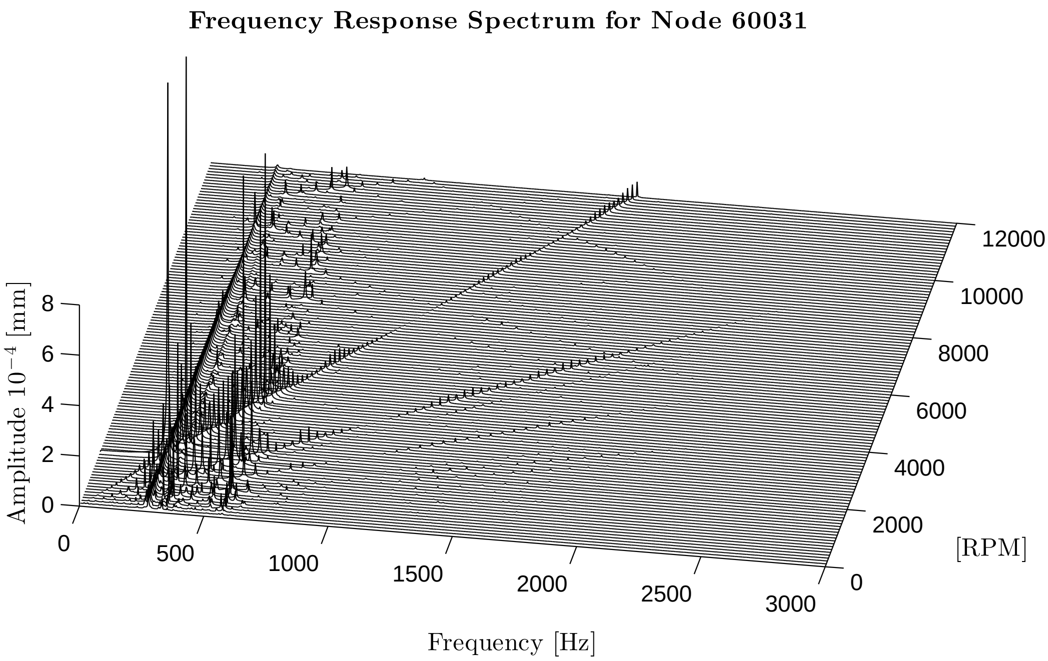

Figure 4.20: Waterfall plot displaying the dynamic response of reference node 60031.

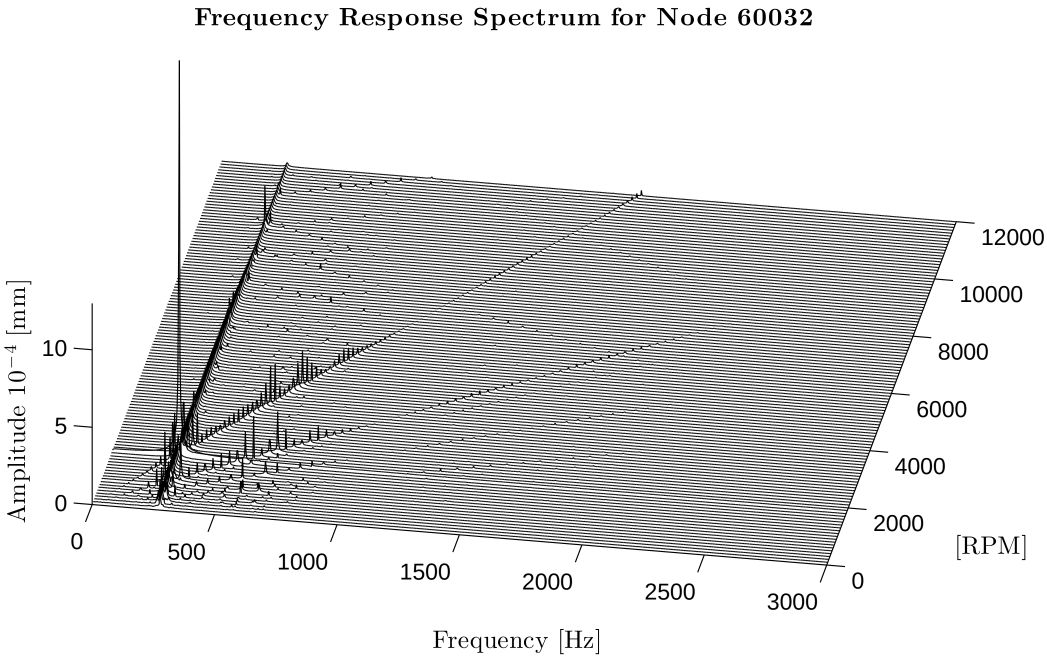

Figure 4.21: Waterfall plot displaying the dynamic response of reference node 60032.

5

Conclusion

5.1 Transmission Errors and Mesh Stiffnesses in Gear Contacts

The results indicate that the magnitude of the transmission error is highly related to the torque applied to the transmission gear drives. This can be seen from the results in Figure 4.1 and Figure 4.3, where the magnitude of the transmission error is reduced as the applied torque is decreased for the higher rotational speeds. The variations in the transmission error for both gear contacts indicate that the variations are also increasing for higher torque loadings. Consequently the magnitudes of the excitations in the gear contacts are increased for the lower rotational speeds in the simulations.

The mesh stiffnesses in both of the gear contacts were found to be decreasing with decreasing torque for the higher rotational speeds. The variations in the mesh stiffness for the first gear contact remained relatively unchanged for the different loadings. For the second gear contact the mesh stiffness exhibited a significant change in behavior for input torques less than circa 102.5 Nm, due to modifications of the micro geometry of the gears resulting in a change of the contact ratio.

5.2 Eigenfrequency Analyzes

From the results of the eigenfrequency analyzes of the individual transmission components, as part of the substructure generation process, it can be concluded that only six of the components eigenfrequencies lied within the examined frequency interval in the dynamic simulations; one for the main shaft, three for the differential, two for the housing and none for the input shaft. It might therefore have been unnecessary to include as many as 20 of the eigenmodes for the substructures. Instead, a frequency interval for the eigenmodes to include could have be specified, rather than a fixed number. For the input shaft the inclusion of the eigenmodes might have been unnecessary and it could instead have been represented only by the mass and stiffness matrix of the substructure.

The eigenfrequencies from the simplified transmission model gave an approximation for which frequencies resonance could be expected for the complete transmission model. The results showed a relatively close resemblance to the eigenfrequencies seen in the waterfall plots for the dynamic response of the housing, however at slightly lower eigenfrequencies compared to the simplified model. This difference can be explained by the increase in stiffness for the simplified model which should result in higher eigenfrequencies for that model. This thereby adds confidence in the model, as it manages to reflect the effects of the eigenfrequencies during the non-linear dynamic simulations.

5.3 Dynamic Response of the Transmission Housing

The results from the dynamic simulations show a clear relationship between the mesh frequencies and their harmonics and the resulting frequency components of the displacement in the transmission housing. This implies that the developed dynamic model manages to simulate the vibrations which from previous studies have been established as the main cause of the gear whine noise. The used solver settings resulted in problems with aliasing when the harmonics of the mesh frequencies reach above 3,000 Hz which is due to a too low sampling frequency. This could be improved by increasing the number of samples and decreasing the size of each time increment. This will however greatly increase the time consumption for the simulations, since the next sample size which can be used for the fast fourier transform is $n = 2^{12} = 4{,}096$. Another approach would be to use the same number of samples but only decreasing the time increments between each sample. This would increase the sampling frequency but instead reduce the resolution of the frequency spectrum according to Equation 2.24.

It should be noted that no damping effects of any sort have been included in the model. The connector elements used for the gear contacts can easily be given damping properties and different methods for adding damping to the transmission components are available in Abaqus®, but determining the appropriate damping coefficients is a difficult process. Adding damping is likely to reduce the time needed for the simulations to reach a steady-state, as damping may reduce the magnitude of the oscillations in the dynamic response.

The proposed dynamic model is relatively simple in its design and could easily be implemented in more complex transmissions involving a higher number of gear contacts. Exporting the calculated transmission errors and mesh stiffnesses from the LDP was done manually for each of the loading cases. This was highly time consuming and it would be advantageous to develop a more efficient extraction method, e.g. write a script performing the extraction. This is of even greater importance if a transmission containing a higher number of gear contacts is examined.

Excitation of the eigenfrequencies of the transmission have been observed, as the amplitudes in the responses are suddenly increased for distinct frequency components, especially 273 Hz, 340 Hz and 550 Hz. The waterfall plots obtained for the dynamic response of the bearing reference nodes of the housing indicates several cases of resonance for rotational speeds below 5,000 RPM, when the mesh frequency harmonics coincide with the eigenfrequencies. Following these results, it would be advisable to design the driveline in such a way that the transmission is operating mainly at rotational speeds above 5,000 RPM. It is especially important to avoid continuous driving conditions to coincide with these rotational speeds which might result in a distinct tonal noise due to the relatively strong vibrations in the transmission housing. The simulations also indicate that the second gear contact is affecting the response to a larger extent than the first gear contact, most likely due to the higher torques being transferred in the second gear contact. Focus regarding optimizing the geometry of the gears should therefore, from a dynamic perspective, lie on reducing the variations in the transmission error in the second gear contact.

The computational time required to obtain a steady-state response is rather great, especially when examining a range of different loading conditions. The average time for one simulation was circa 1h and 22 min which results in a total time for all 120 simulations of approximately 163 h and 20 min. The use of a non-linear bearing model for calculating the stiffness of the bearings is a contributing cause of the relatively time consuming simulations, as it has to iterate in every time increment in order to obtain a new bearing stiffness matrix. One alternative could be to use the resulting bearing stiffness matrices after the static step and then use these throughout the dynamic steps. This would reduce the time consumption but change the results, but to what extent is unclear.

The developed dynamic model and simulation methodology should mainly be used in order to evaluate and compare different proposals regarding the design of the transmission housing. Thorough testing by experiments performed on a physical model of the transmission has to be performed in order to evaluate whether or to what extent the proposed dynamic model manages to represent the actual dynamic behavior of the transmission.

5.4 Future Work

As mentioned above, experiments and methodology for validating the developed dynamic model are necessary in order to establish the accuracy of the model. It would also be interesting to compare the results of the dynamic response for different mode addition methods, e.g. using the Craig-Chang method or the mixed-interface method when including eigenmodes in the substructures. By adding additional retained nodes positioned on the surface of the housing, instead of just using the bearing reference nodes, a better analysis of the noise generating vibrations could be performed. This would allow for a higher geometric resolution of the dynamic response of the housing. It would also be favorable to develop methods for estimating the magnitude of the resulting sound generated by the simulated vibrations in the transmission housing. In addition to adding damping, effects of backlash could be introduced in the gear contacts. This has been proposed in previous works, e.g. [19] and could further refine the model.

Bibliography

[1] D. Houser, J. Harianto, Y. Ueda, Determining the source of gear whine noise, `http://www.gearsolutions.com/media//uploads/assets/PDF/Articles/2004-02-01_Determining_the_Source_of_Gear_Whine_Noise.pdf`, [Accessed 10 September 2012] (2004).

[2] S. Curtis, J. Pears, D. Palmer, M. Eccles, A. Poon, M. Kim, G. Jeon, J. Kim, S. Joo, An analytical method to reduce gear whine noise, including validation with test data, SAE Technical Paper 01 (1819) (2005) 1–10.

[3] J. Smith, Gear Noise and Vibration, Marcel Dekker, Inc, New York, 2003.

[4] R. Gregory, S. Harris, R. Munro, Dynamic behaviour of spur gears, Applied Mechanics Group 178 (8) (1962) 207–221.

[5] R. Singh, A. Kahrman, Non-linear dynamics of a spur gear pair, Journal of Sound and Vibration 142 (1) (1990) 49–75.

[6] S. Harris, Dynamic loads on the teeth of spur gears, Proceedings of the Institution of Mechanical Engineers 172 (1958) 87–112.

[7] M. Beacham, D. Bell, N. Powell, Development of transmission whine prediction tools, SAE Technical Paper 01 (1767) (1999) 1–12.

[8] C. Chung, G. Steyer, Gear noise reduction through transmission error control and gear blank dynamic tuning, SAE Technical Paper 01 (1766) (1999) 1–10.

[9] B. Hamrock, B. Jacobson, S. Schmid, Fundamentals of Machine Elements, McGraw-Hill, 1999, pp. 613–657.

[10] M. Mägi, K. Melkersson, Lärobok i Maskinelement, EcoDev International, Göteborg, 2008, pp. 412–494.

[11] D. B. Marghitu, Kinematic Chains and Machine Components Design, Academic Press, Waltham, Massachusetts, 2005, pp. 639–646.

[12] M. Åkerblom, Gear noise and vibration - influence of gear finishing method and gear deviations, Licentiate thesis, Royal Institute of Technology, Stockholm (2002).

[13] H. Özgüven, D. Houser, Dynamic analysis of high speed gears by using loaded transmission error, Journal of Sound and Vibration 125 (1) (1988) 71–83.

[14] W. Tuplin, Gear-tooth stresses at high speed, Proceedings of the Institution of Mechanical Engineers 163 (1950) 162–175.

[15] Y. Wu, J. Wang, Q. Han, Contact finite element method for dynamic meshing characteristics analysis of continuous engaged gear drives, Journal of Mechanical Science and Technology 6 (26) (2012) 1671–1685.

[16] M. Friswell, J. Penny, S. Garvey, A. Lees, Dynamics of Rotating Machinery, Cambridge University Press, 32 Avenue of the Americas, New York, NY 10013-2473, USA, 2010.

[17] R. Singh, D. Houser, A. Kahraman, Non-linear dynamic analysis of geared systems, Technical Report 90-C-020, NASA (1990).

[18] H. Özgüven, A non-linear mathematical model for dynamic analysis of spur gears including shaft and bearing dynamics, Journal of Sound and Vibration 145 (2) (1991) 239–260.

[19] C. Siyu, T. Jinyuan, L. Caiwang, W. Qibo, Nonlinear dynamic characteristics of geared rotor bearing systems with dynamic backlash and friction, Mechanism and Machine Theory 46 (4) (2011) 466–478.

[20] G. Liu, Nonlinear dynamics of multi-mesh gear systems, Dissertation, The Ohio State University (2007).

[21] Dassault Systèmes, Abaqus Analysis User's Manual (2011).

[22] R. Craig Jr., A. Kurdila, Fundamentals of Structural Dynamics, 2nd Edition, John Wiley & Sons Inc., Hoboken, New Jersey, 2006.

[23] L. Houpert, A uniform analytical approach for ball and roller bearings calculations, ASME Journal of Tribology 119 (4) (1997) 851–858.

[24] J. Harianto, D. Houser, User's Manual for Load Distribution Program LDP, The Ohio State University, 206 West 18th Avenue, Columbus, OH 43210, USA, 10th Edition (May 2002).